# Cortical layer-specific modulation of neuronal activity after sensory deprivation due to spinal cord injury

**Marta Zaforas[1,2,3], Juliana M. Rosa[1,3], Elena Alonso-Calviño[1], Elena Fernández-López[1], Claudia Miguel-Quesada[1], Antonio Oliviero[2], Juan Aguilar[1,4*]**

[1]Experimental Neurophysiology and Neuronal Circuits Group, Research Unit, Hospital Nacional de Parapléjicos. SESCAM, Toledo, 45071 Spain.

[2]FENNSI Group, Research Unit, Hospital Nacional de Parapléjicos. SESCAM, Toledo, 45071 Spain.

[3]These authors contributed equally

[4]Lead Contact

[*] Corresponding author: jdaguilar@sescam.jccm.es

## Summary

Cortical areas have the capacity of large-scale reorganization following sensory deprivation. However, it remains unclear whether this is a unique process that homogenously affects the entire deprived region or it is suitable to changes depending on local circuitries across layers. By using *in vivo* electrophysiology to record neuronal activity simultaneously across cortical depth, we showed that sensory deprivation due to spinal cord injury induces layer-specific changes in both spontaneous and evoked-activity. While supragranular layers specifically increased gamma oscillations and the ability to initiate up-states during spontaneous activity, infragranular layers displayed increased, faster and delayed evoked-responses to sensory stimulation. Therefore, sensory deprivation immediately modifies local circuitries allowing supragranular layers to better integrate spontaneous corticocortical information to maintain column excitability, and infragranular layers to better integrate evoked-sensory inputs to preserve subcortical outputs. These layer-specific changes may guide long-term alterations in excitability and plasticity associated to network rearrangements and the appearance of sensory pathologies associated with spinal cord injury.

## Introduction

Spinal cord injury (SCI) produces an abrupt and robust loss of sensory inputs onto cortical areas that receive information from body regions below the lesion level (i.e. hindlimb cortex that receives afferent inputs from hindlimbs). This sensory deprivation initiates the so-called process of cortical reorganization (CoRe), which is typically described as an expansion of the neuronal activity from intact cortical areas towards the sensory deprived cortex (Curt et al., 2002; Endo et al., 2007; Ghosh et al., 2010; Jain et al., 1998, 2008; Chand and Jain, 2015). CoRe plays key roles in the functional recovery after SCI, but it has also been implicated in the generation of associated pathologies such as neuropathic pain and spasticity (Gustin et al., 2010; Peyron et al., 2004; Siddall et al., 2003; Wrigley et al., 2009). Similar cortical rearrangements after sensory deprivation have also been described in different sensory systems as visual (Griffen et al., 2017; He et al., 2006) and auditory cortex (Bola et al., 2017). Most of studies about cortical reorganization after SCI have used large-scale experimental approaches such as extracranial electroencephalographic recordings (Green et al., 1998), voltage sensitive dye (Ghosh et al., 2010) and functional magnetic resonance imaging (Endo et al., 2007) in a period ranging from days-to-months after the injury. However, it is currently known that such functional changes are observed immediately after SCI in different animal models as rodents (Aguilar et al., 2010; Humanes-Valera et al., 2013; Yagüe et al., 2014; Yague et al., 2011) and pigs (Jutzeler et al., 2019). In this line, our group have previously shown that both intact and deprived somatosensory cortex became more responsive to peripheral sensory stimulation above lesion level few minutes after the lesion (Humanes-Valera et al., 2013; Yagüe et al., 2014), while spontaneous activity is drastically reduced (Aguilar et al., 2010; Fernández-López et al., 2019). In addition to the cortical changes, SCI also modifies thalamic and brainstem spontaneous and evoked neuronal excitability, which may be linked to the changes observed in the somatosensory cortex (Alonso-Calviño et al., 2016; Dutta et al., 2014; Jain et al., 2000, 2008; Liang and Mendell, 2013).

Changes in the cortical activity after SCI have been mostly studied by using electrophysiological recordings from layer 5 neurons. However, the neocortex is a complex structure composed of six layers organized in distinct vertical columns. Within each layer, different functional properties and

input/output connections are achieved by interconnected excitatory pyramidal neurons, inhibitory neurons, and glial cells (Bayraktar et al., 2020; Derdikman et al., 2006; Fiáth et al., 2016). Although several studies in the last decade have shed light into distinct strategies used by each layer to encode information, less is known about the functional changes induced within each cortical layer following sensory deprivation that may precede long-term cortical reorganization and could help to understand the physiological changes in brain areas controlling the integration and processing of sensory inputs.

Using *in vivo* electrophysiological recordings from anesthetised rats, we studied how neuronal activity mediated by corticocortical and thalamic connections as well as local circuitries in the hindlimb cortex (HLCx) are immediately affected by sensory deprivation after a thoracic SCI. For that, we used a vertical multielectrode array to determine the neuronal excitability across layers of the deprived HLCx during evoked and spontaneous activity. Peripheral stimulation of the contralateral forelimb showed a layer-dependent increase in sensory evoked-LFP responses across HLCx layers indicating that changes in neuronal network properties of the deprived cortical column may favour the excitability. However, a striking heterogeneity was observed when other physiological parameters were analysed. Infragranular L5/6, but not L2/3, exhibited increased LFP slope, increased multiunit activity and delayed onset latencies. On contrary to evoked-responses, spontaneous activity was mostly affected in supragranular layers as observed by increased high-rhythms frequencies and probability to initiate UP-states. Altogether, our data indicate that SCI immediately modifies local circuitries within the deprived cortex allowing supragranular layers to better integrate spontaneous corticocortical information, thus modifying the excitability of the column, and infragranular layers to better integrate evoked-sensory inputs to preserve subcortical outputs.

## RESULTS

### *Laminar analysis of evoked neuronal responses in the somatosensory cortex following peripheral stimulation*

We first characterized the evoked-local field potentials (evoked-LFP) across layers of the HLCx in response to sensory stimulation delivered either to the contralateral hindlimb (HL) or forelimb (FL) in intact anaesthetised animals (Fig. 1). For that, we used a linear 32-multielectrode probe inserted vertically into the HLCx such that recording sites were located across all layers in a single column to simultaneously record LFPs and local multiunit activity (MUA). Figure 1A shows a schematic representation of the recording location and stimulation paradigm as well as a histological preparation showing an electrode track into HLCx (Fig. 1B). Representative examples of averaged evoked-LFPs across the entire depth of HLCx in response to a 5 mA hindlimb stimulation (0.5 Hz) is shown in the left panel of Figure 1C. Note that a high intensity stimulation was chosen to maximize the activation of peripheral nerves to ensure the full engagement of cortical circuits involved in somatosensory processing (Lilja et al., 2006). The laminar profile of averaged LFP responses of the population obtained by hindlimb stimulation showed a clear difference in the response magnitude across the cortical depth, with a maximum peak at distances from surface between 700-1000 µm corresponding to the thalamorecipient granular layer 4. No differences were observed using low intensity stimulation, which resembles light mechanical stimuli that preferentially activates dorsal column pathways (Lilja et al., 2006). Current source density (CSD) analysis was overlapped to LFP traces to determine the entrance of synaptic inputs in different cortical layers (Fig. 1C, heat map) showing an evident current sink (inward current) in L4. The active sink was surrounded by two strong current sources (outward current), one short-lasting in L2/3 and another long-lasting in infragranular layers (L5 and L6). A small and elongated current sink was also observed in L6, which may refer to the thalamocortical loop initiated by evoked responses. The greater LFP response magnitude and the current sink at the thalamorecipient L4 corroborate the correct location of the electrode at the somatotopic representation of hindlimbs. Finally, MUA responses (Fig. 1D, left panel) were analysed by rectifying the neuronal firing (rMUA) obtained in response to peripheral stimulation at high and low intensities (Fig. 1D, right panel). The area of the evoked-rMUA showed robust neuronal firing in the upper infragranular layer (i.e. L5), while L2/3 and L6 neurons showed low and sparse firing response. A similar laminar profile of neuronal responses was observed using low intensity stimulation (0.5 mA).

We next examined the pattern of cortical responses when the peripheral stimulation was applied to an adjacent, non-corresponding somatotopic body region, i.e. recording in HLCx, while stimulating forelimb afferents. Figure 1E

shows LFP representative traces produced in the HLCx in response to high intensity electrical stimulation of contralateral forelimb. Despite of the small amplitude, evoked-LFP responses were clearly observed across all recording channels with infragranular layers showing the highest magnitude. Similar results were also observed using 0.5 mA stimulation indicating a strong HL-FL cortical connectivity even to low intensity stimuli. In response to high stimulation, rMUA in infragranular layers showed a clear evoked activity with a peak in layer 6, while L2/3 and L4 exhibited only sparse and very low response. Therefore, our data indicate that each cortical layer exhibits a characteristic neuronal activity in response to stimulation of its own receptive field as shown in previous studies (Wilent et al., 2004; Sakata and Harris, 2009), but also in response to non-preferential peripheral stimulation (i.e. neuronal activity in HLCx in response to forelimb stimulation) which evidences a heterogenic cortical excitability most probably due to the composition of each local circuitry and synaptic inputs.

### *SCI induces layer-dependent functional changes in the sensory deprived cortex*

Given the layer-specific activity induced in the HLCx in response to forelimb stimulation under control conditions, we hypothesised that SCI should induce specific effects on the evoked-LFP in a layer-dependent manner. To explore that, we investigated the neuronal activity across cortical layers immediately after sensory deprivation due to SCI in 24 rats (Fig. 2). As expected, an abolishment of the evoked-LFP was immediately observed in all layers of the HLCx in response to hindlimb stimulation, confirming the complete loss of sensory inputs (Fig. 2A). When peripheral stimulation was applied to the contralateral forelimb, the magnitude of evoked-LFP produced in HLCx were significantly increased in all layers but L6 (Fig. 2B, repeated measures ANOVA, SCI $F_{(1,91)} = 50.2$, $p < 0.001$), indicating heterogeneous immediate changes in the excitatory post-synaptic activity of local pyramidal neurons and/or in the strength of arriving synaptic inputs. Next, we examined the area of the rectified MUA as a measure of local neuronal activity in each cortical layer recorded in a subset of SCI animals (16 out of 24 SCI animals; Fig. 2C). Figure 2D shows examples of evoked rMUA from each channel superimposed on a colour-coded map from the same animal in response to high intensity stimulation (5 mA) before and after SCI. Two-way analysis of variance of our data showed significant differences for layers ($F_{(3,60)} = 12.5$, $p < 0.001$), and SCI condition ($F_{(1,60)} = 18.1$, $p < 0.001$), but no interaction between layers and SCI ($F_{(3,59)} = 1.2$, $p = 0.31$). Before SCI, L2/3 and L4 neurons exhibited very low activity, while robust firing was observed only in L5 and L6 in response to forelimb stimulation. After SCI, neuronal firing tended to increase in all layers (see original traces in Fig. 2E), with L5 rMUA significantly increased post-lesion ($p < 0.05$). These results demonstrate that immediate sensory deprivation due to SCI produces increased neuronal firing in infragranular layers, and importantly creates differences in neuronal excitability among cortical layers of the deprived HLCx. Due to the non-consistent responses obtained among individuals when low intensity stimulation was applied, herein, data were considered only for responses obtained to high intensity stimulation in forelimb (5mA).

Previous data obtained from human studies have shown that changes in cortical activity are not homogenous across SCI patients (Wrigley et al., 2009; Freund et al., 2013; Jutzeler et al., 2015). Therefore, we hypothesised that immediate cortical deafferentation could affect non-uniformly to individuals in the studied population, and more specifically that a subset of our experimental animals may not exhibit the overall changes in the neuronal cortical activity following immediate SCI. To explore whether such assumption was true, we plotted the individual values corresponding to the ratios between the evoked-LFP response post and pre SCI obtained from layer 5 neurons for each studied animal (Fig. 2F). Note that layer 5 was chosen due to the large responses following forelimb stimulation and the significant effect previously described after SCI (Humanes-Valera et al., 2017; Fernández-López et al., 2019). This allowed us to identify a clear separation of animals in which SCI induced increments in the magnitude of the evoked-LFP (ratio > 1, 19/24 animals (79 %)), from those animals in which LFP amplitude remained stable or even decreased (ratio < 1, 5/24 animals (21 %), Fig. 2F). A parallel representation of the evoked-LFP and rMUA following SCI within each group is shown in Sup. Figure 1A-D. Note that statistical differences among layers between pre and post SCI remain similar to those observed when using all experimental data, demonstrating that the groups did not distort our results statistics and are inherently independent of the selection criteria (Kriegeskorte et al., 2009; Makin and Orban de Xivry, 2019). Therefore, our results strongly suggest that SCI immediately increase the excitability of deprived neurons in a layer-specific manner. Moreover, we observed that immediate cortical deprivation does

not affect homogeneously to all subjects of a population that could be clustered in affected and non-affected subsets.

### *SCI strongly affects the corticocortical and thalamocortical connectivity between infragranular layers*

Once we determined that SCI distinctly affected cortical layers and individuals, we sought a deep characterization of the functional alterations produced in the deprived HLCx in response to forelimb stimulation in both group of animals. It has been proposed that increased cortical responses after SCI could be mediated by a reduction of inhibitory activity that consequently unmask latent excitatory inputs of sensory deprived region, therefore modulating the dynamics of local responses (Sydekum et al., 2014). Taking this assumption into account, our proposed hypothesis was that sensory deprivation would differently affect the kinetics of LFP produced at each cortical layer based on the different inhibitory tone relieved at local neuronal network. Thus, we first analysed the slope values (decay rate in mV/s) of evoked-LFP that are often used to determine changes in the arrival and/or synchronization of synaptic inputs and are usually affected by changes in the excitation:inhibition balance (Fig. 3A). Under control conditions, hindlimb stimulation induced fastest responses in L4 of the HLCx (Fig. 3B), while forelimb stimulation induced similar slope values across all layers (Fig. 3C). After SCI, slope values significantly increased in HLCx L4 and infragranular layers in response to forelimb stimulation in Group 1, but not in Group 2 animals (Fig. 3C). The fastest rising slope was observed in L6 indicating a strong recruitment of neuronal population after SCI as can be observed by a shorter time-to-peak values (Fig. 3D).

Next, we determined the response latencies for each electrode site and for spatially averaged responses within electrodes from the same layer to create a spatiotemporal profile of the response onset (Fig. 4). Onset responses from LFP and rMUA were obtained by fitting a sigmoid function to the data and then computing the maximum curvature as described in Fedchyshyn and Wang, 2007 (see Methods). Figure 4A-B shows an example of laminar LFP profile and averaged onset latencies obtained from HLCx in response to hindlimb stimulation in control conditions. In this case, activity originated in upper middle layers and spread upwards and downwards resembling the propagation of evoked activity typically seen in distinct cortices (Sakata and Harris, 2009; Schroeder et al., 1998). Next, we analysed the evoked-LFP onset in response to forelimb stimulation, which could indicate how the corticocortical connectivity between HL-FL cortices is organized. In both groups of animals (Fig. 4C-D pre-SCI, Sup. Fig. 1E), averaged onset was found to be similar across all layers with higher probability to be initiated in infragranular layers. These data indicate that population activity measured as LFP in response to peripheral forelimb stimulation reaches HLCx almost simultaneously as previously reported using voltage-sensitive dyes (Wester and Contreras, 2012). Such pattern of activity onset was strongly affected by sensory deprivation in a layer-dependent manner. Infragranular layers presented a significant delay in the onset of the evoked responses, while onsets in granular and supragranular layers were not affected (Fig. 4C-D post SCI). In addition, onset probability was also similar across layers after SCI. We then analysed the onset pattern of the evoked rMUA (Fig. 4E). Before SCI, HLCx infragranular layers exhibited faster onset latencies than supragranular layer with neuronal firing originating mostly in infragranular 6. After SCI, differences in onset responses disappeared due to rMUA of infragranular tend to be delayed (Fig. 4E).

### *SCI induces delayed thalamocortical inputs to the deprived cortex*

A possible mechanism leading to the delayed LFP and rMUA onsets in infragranular layers would be that SCI induces changes in the two main neuronal pathways that drive the peripheral information from forelimbs to HLCx: 1) a canonical corticocortical pathway in which synaptic inputs from the thalamic forelimb region routes to FLCx and then reaches HLCx mostly through L2/3 (FL-Th→FLCx→HLCx); and 2) a non-canonical thalamocortical pathway involving the activation of a subset of HL neuronal population in the thalamus that project to HLCx in response to forelimb stimulation, HL-Th→HLCx (Figure 5A; Alonso-Calviño et al., 2016; Francis et al., 2008). Considering that delayed onset was observed in both HL and FL thalamus immediately after SCI (Alonso-Calviño et al., 2016), we wanted to determine which thalamocortical pathway was the most plausible to be involved in the delayed HLCx evoked-responses. To prove this idea, we have analysed simultaneous electrophysiological recordings from FLCx and HLCx obtained from tungsten electrodes located on layer 5 of both cortical regions under control conditions and after SCI (Fig. 5B, these data were obtained simultaneously to thalamic data that were published in Alonso-Calviño et al., 2016). We postulated that if increased response latencies of HLCx after SCI were induced by changes in the

canonical pathway, then synaptic inputs would arrive earlier at the FLCx than at HLCx. On the other hand, if non-canonical pathway produces the longer latency of HLCx evoked responses, then both cortical regions should exhibit similar latencies after forelimb stimulation. Our results demonstrated that both the intact FLCx and the sensory deprived HLCx showed similar increased latencies to peripheral FL stimulation immediately after SCI with no differences between them (Fig. 5C, $p > 0.05$). Therefore, increased latency of cortical evoked responses could be at least in part due to longer latencies that take place in thalamic VPL corresponding to HL and FL as we described in Alonso-Calviño et al. 2016. Moreover, we cannot discard other intrinsic properties or corticocortical mechanisms involved in this process.

### *Spontaneous activity is determined by cortical layer properties under control conditions and after sensory deprivation*

Cortical spontaneous activity in anesthetized animals is generally dominated by slow-wave activity (SWA, Fig 6A). SWA is mainly originated from local neuronal networks and corticocortical connections (Chauvette et al., 2010; Sanchez-Vives and McCormick, 2000) and is importantly modulated by sensory inputs reaching the cortex throughout thalamic pathways (David et al., 2013; Rigas and Castro-Alamancos, 2009). In this context, we have previously demonstrated that the drastic sensory loss after SCI reduces the neuronal excitability during cortical SWA (Aguilar et al., 2010; Fernández-López et al., 2019). As these data were obtained from deprived HLCx layer 5 neurons and SWA up-states propagate vertically across layers *in vitro* and *in vivo* (Sakata and Harris, 2009; Sanchez-Vives and McCormick, 2000), we thus calculated the onset of the spontaneous activity to determine the pattern of vertical propagation in our experimental conditions from Group 1 animals. Before SCI, spontaneous up-states initiated in any cortical layers (Fig. 6B), with infragranular layers 5 and 6 showing the highest onset probability (~80%), which corroborates previous findings in somatosensory cortex of anesthetized rats (Fiáth et al., 2016; Sakata and Harris, 2009). After SCI, we found that although spontaneous up-states also tend to start in infragranular layers, this probability decreased to ~60%. This effect was achieved by a parallel increase in the probability of up-states starting at L2/3 (Fig 6B). By analysing the rate of neuronal activity transfer across layers, we observed that up-states originated in L2/3 propagated downwards in similar velocities before and after SCI (Fig. 6C-D, control 38.7 ± 8.6 μm/ms, SCI 36.8 ± 11.2 μm/ms), whereas spontaneous activity originated in deep layers propagated upwards in a velocity rate much slower after SCI than in control conditions (Fig 6E-F, control 39.2 ± 10.4 μm/ms, SCI 27.52 ± 12.1 μm/ms, $p < 0.01$). These data indicate that SCI induced immediate changes in the neuronal network of deprived cortical column that slow-down the propagation of spontaneous activity originated in infragranular layers. In addition, they also showed an increased probability of spontaneous up-states initiated in L2/3, most probably through corticocortical connections between HL-FL that helps to propagate spontaneous activity from the adjacent FL cortex.

Changes in the generation of spontaneous activity may indicate that other cortical features could be affected by SCI. Following this idea, we considered that alterations of intrinsic excitability should also be reflected in the frequencies content of the LFP signal in each layer during spontaneous activity from Group 1 animals (Fig. 7). Spectrogram analysis performed on individual traces from L2/3, L4 and L5/6 layers (exampled red traces on Fig. 7A) confirmed the presence of slow (0.1-9 Hz) and fast rhythms (10-80 Hz) during up-states before SCI (Fig 7B). Interestingly, our spectrogram analysis showed an increased relative power of fast rhythms mainly in supragranular layers following immediate SCI. Changes in the internal frequencies within up-states after SCI can be clearly observed by the fast oscillations (band pass filtered 25-80Hz) shown in the original traces in Figure 7C (lower traces). To explore such frequency differences in a systematic manner, we performed a power spectrum analysis of the LFP frequencies that were divided into SWA (0.1-1 Hz), delta (1-4 Hz), theta (4-8 Hz), alpha (8-12 Hz), beta (12-25 Hz), low gamma (25-50 Hz) and high gamma (50-80 Hz). Our data showed that from all the studied frequency bands, the relative power of the high gamma was consistently increased in supragranular layers following a SCI (Fig. 7D). The rest of the studied frequency bands were not altered by SCI as summarized in Supplemental Table 3. Therefore, a massive sensory loss produced by an immediate SCI affects differently to of intrinsic excitability of cortical layers characterized by lower ability of layer 5 to generate up-states and increased gamma frequency in supragranular layers during spontaneous activity.

## DISCUSSION

Here we investigated the immediate effects that a robust sensory deprivation induces in distinct layers of the primary somatosensory cortex. Our study gives strong evidence that acute SCI induces layer-dependent changes in local circuits mediating evoked and spontaneous activity in the deprived cortical region through alterations of both corticocortical and thalamocortical connections. Regarding evoked responses, sensory deprivation potentiated the response magnitude and the rising of the population neuronal activity of infragranular layers (L5/6) of the deprived HLCx. On the other hand, the study of spontaneous activity show that supragranular layer 2/3 is the most affected by SCI exhibiting increased probability to initiate spontaneous up-states and increased power of high-frequency oscillations in the gamma band spectrum. Therefore, our results show that local neuronal and network properties of each cortical layer are responsible for differential effects observed in the deprived somatosensory cortex after SCI.

### *Layer-dependent changes in sensory-evoked responses after SCI*

Sensory deprivation has dramatic effects on the organization of brain circuitries, leading to a takeover of the deprived cortex by other cortical areas. This process is initiated as soon as deprivation occurs (Han et al., 2013; Humanes-Valera et al., 2013) and continues in a time scale from days-to-months (Endo et al., 2007; Sydekum et al., 2014; Humanes-Valera et al., 2017; Fernández-López et al., 2019). In the case of SCI, the reorganization of the deprived cortex leads to the acquisition of new sensory functions that could help functional recovery (Rossignol and Frigon, 2011) as well as initiates associated pathologies as pain and spasticity (Siddall and Loeser, 2001). The mechanisms driving beneficial or detrimental reorganization are unknown, but it could rely on the complex laminar organization of cortical areas known to have distinct cellular composition and intrinsic circuitries. Therefore, a better knowledge of the contribution of each cortical layer to the well-known phenomenon of CoRe after sensory deprivation is required. In this study, we have included for the first time the perspective of cortical layering role in the cortical changes after SCI, which could explain initiation and complexity of CoRe as well as explain the variability between individuals as observed in human patients.

Previous differences among layers were only addressed in a neonatal SCI model in which the effects of exercise in the cortical long-term plasticity were studied (Kao et al., 2009). Our present data goes further to demonstrate that neuronal activity is differentially affected across layers of the sensory-deprived HLCx immediately after a SCI in adult individuals. Under our experimental conditions, increased magnitude of evoked-LFP in response to stimulation of the contralateral forelimb was observed across layers of the deprived cortex, which is very consistent with results obtained using brain scanning approaches (Endo et al., 2007; Ghosh et al., 2010). This effect could be explained by the anatomical and functional overlapping of hindlimb and forelimb cortical areas (Moxon et al., 2008; Kao et al., 2009; Morales-Botello et al., 2012), in which corticocortical excitatory inputs may became unmasked following SCI and increase the responses to stimulation of a non-corresponding extremity (i.e. forelimb). In addition, we have previously shown that SCI increases neuronal responses in the thalamic hindlimb region to forelimb stimulation (Alonso-Calviño et al., 2016). Therefore, changes in thalamic excitability could also play a direct role in the increased cortical responses of sensory deprived HLCx. The initial slopes of evoked-LFP, often used to determine changes in the arrival and/or synchronization of synaptic inputs and are usually affected by changes in the excitation:inhibition balance, were significantly faster in granular and infragranular neurons. Since cortical layers are known to display different inhibitory features (Wilent and Contreras, 2004), our data showing changes in the LFP slope in a layer-dependent manner suggest that local network properties are differentially affected by SCI and could represent an unequal reduction of local inhibition across layers allowing infragranular cells to better integrate evoked-sensory inputs.

Onsets of evoked-sensory responses in cortical regions are driven by synaptic inputs from corticocortical and thalamocortical connections. Our data showing almost simultaneous initiation of evoked responses between layers (Fig. 4C-D) corroborates *in vitro* data showing that horizontal corticocortical connectivity with adjacent cortical areas induces similar onsets of evoked responses (Wester and Contreras, 2012). However, this feature was strongly delayed in L5/6 of the deprived cortex after SCI, which could indicate modifications in the cortico-cortical synaptic connectivity but also in thalamic connections that project to HLCx. *In vivo* peripheral forelimb stimulation induces strong neuronal responses in the FL area of the thalamic VPL, but also in a population of the HL area of the VPL through collaterals that finally project onto HLCx (Fig. 5A,Alonso-Calviño et al., 2016). By

simultaneously recording neuronal activity in HLCx and intact FLCx we showed that SCI leads to a delayed latency in the neuronal activity of both regions in response to peripheral stimulation. In addition, we did not observe changes in the onset of thalamus-devoid supragranular neurons after SCI, suggesting that the onset of evoked-LFP responses in infragranular layers is more conditioned by changes in thalamic inputs. Therefore, our data indicate that although a delay in the arrival of synaptic inputs in infragranular layers is observed after SCI, these are more efficiently integrated as showed by increased slope and magnitude of evoked-LFP. Then, sensory deprivation produces changes in the integration properties of local networks of the deprived infragranular neurons that could be the basis for the long-term reorganization of sensory cortex observed after SCI.

Electrophysiological recordings of LFP and action potentials reflect different but complementary aspects of neuronal processing (Buzsáki et al., 2012). While LFP integrates subthreshold activity as synaptic inputs and membrane potentials from a neuronal population in a given region, action potentials are the output signals from individual neurons close to the recording electrode. Contrary to the homogeneous increase in the evoked-LFP after SCI through L2/3-L5, we found striking differences among layers regarding MUA. In this case, sensory deprivation increased neuronal excitability in infragranular neurons of the deprived HLCx but not in granular and supragranular layers. Infragranular neurons have several characteristics that may lead to most of the changes: they receive excitatory inputs from all other cortical layers and neighbouring cortical areas (Schubert et al., 2007), they receive extensive thalamic inputs, and they have larger receptive fields (Moxon et al., 2008; Rigas and Castro-Alamancos, 2009; De Pasquale and Sherman, 2011; Wester and Contreras, 2013). Therefore, changes in the local network connectivity and/or intrinsic properties of infragranular neurons are more prone to be noticed after SCI compared to other layers. Moreover, the only intracellular data obtained from infragranular neurons after acute SCI (Humanes-Valera et al., 2017) perfectly support the relation between the increased MUA responses and the faster slope of evoked-LFP that we show in the present work. Altogether our data strongly indicate that excitability of infragranular neuronal networks are mostly affected in the context of evoked responses, which could be directly implicated in the mechanisms regulating subcortical output generating adaptive behaviour and functional recovery following spinal cord injury.

Our data also identified a subset of animals (21%) that consistently didn't show immediate neuronal changes related to neither evoked responses nor spontaneous activity. Interestingly, population studies comparing neuronal activation in SCI patients with those in health individuals have constantly shown several degrees of cortical "expansion" towards the deafferented brain region and cortical activity in the deprived area with divergent results regarding the appearance of neuropathic pain (Moxon et al., 2014; Wrigley et al., 2018). Similar results are also observed in amputees in which phantom limb pain has been either associated with a stronger representation of the missing body part and maintenance of its structural integrity (Makin et al., 2013; Makin et al., 2015) or a remapping of the cortical areas (Flor et al., 1995). It is thought that the degree of cortical reorganization can be attributed to several variables including species, age, behavior activity and therapies regimes after the injury (Moxon et al., 2014; Jutzeler et al., 2019). Since we did not find any differences regarding age, sex or anatomical location of the electrode, we postulate that the population that did not exhibit changes in the cortical activity may result from our acute model of SCI (i.e. from minutes to few hours), which does not exclude the possibility that these animals present cortical changes in sub-acute and/or chronic phases of the injury. In addition, it would be interesting in future to determine whether such small population is directly linked, or not, to sensorimotor pathologies usually observed after SCI. Although our main results are supported by the consistent effects observed in the 79% of animals with SCI that we have studied, we found these results very important as they increase the variability and heterogeneity of effects observed in individuals with SCI, which should be taken into account in the context of cortical reorganization.

***Sensory deprivation affects the generation of gamma oscillations and the propagation of Up-states in the cortical column.***

In our experimental model, the cortical activity before SCI was settle to the state of slow-wave oscillation (~1 Hz) characterized by alternating periods of synchronized activation of neuronal population (up-states) and silent periods (down-states; Steriade et al., 1993). Up-state events are dominated by gamma frequency activity (25-80 Hz) with implications in multiple aspects of information processing such as sensory representation (Castro-Alamancos, 2009), sensorimotor integration (Schoffelen et al., 2011) and cognition (Gruber et al., 2004). Here, we describe that sensory deprivation

due to SCI induces a layer-specific modulation of high frequency oscillations during Up-states, with gamma range being strikingly increased in supragranular layers, but not in infragranular or granular layers. Layer 2/3 is known to present a network of inhibitory neurons that initiates gamma-oscillations either through PV-neurons (Cardin et al., 2009; Welle and Contreras, 2016) or somatostatin neurons (Veit et al., 2017). In this context, the sensory deprivation produces a reduction in the constant thalamic excitatory inputs onto the deprived cortex that may lead to an increase of the general inhibitory tone in supragranular layers, which facilitates local mechanisms of gamma oscillations. In addition to the well-described role of high frequencies in information processing, gamma oscillations have also been implicated in the formation of cortical maps during development (Minlebaev et al., 2011) and related to generation of pain perception in somatosensory cortex (Tan et al., 2019). Therefore, it is plausible that the increased gamma may be related with several long-term physiological changes observed following SCI such as cortical reorganization linked to functional recovery as well as maladaptive plasticity linked to chronic pain. Moreover, this neuronal feature could also be used as a functional biomarker for CoRe after a CNS injury, as previously shown in human auditory cortex after noise trauma (Ortman et al., 2010).

Spontaneous up-states within slow-wave oscillations usually initiate in deep infragranular layers (Sakata and Harris, 2009) and depend primarily on both intrinsic properties of the cortical column and corticocortical connections (Sanchez-Vives and McCormick, 2000; Timofeev et al., 2000). Our data shows that SCI induces a 1-fold increase in the probability of up-states generation in layer 2/3 with a consequent decrease in layers 5/6. There are several possible mechanisms that both isolated or synergistically could be leading to such changes. First, subthreshold oscillations in the membrane potential during gamma oscillations facilitate the generation of spontaneous up-states (Kuki et al., 2015, Puig et al., 2008). Since we also observed increased gamma in L2/3 after SCI probably due to increased activity of inhibitory neurons, this mechanism could be a trigger to the increased up-state onset (Compte et al., 2003). Second, we have previously shown that SCI decreases neuronal activity during up-states in layer 5 neurons (Fernandez-Lopez et al., 2019), which may favour the initiation of up-states in layer 2/3 by releasing supragranular neurons from L5 to L2/3 modulation (Wester and Contreras, 2012). In the same way, *in vitro* experiments show that up-states generation in the somatosensory cortex is reduced after blocking thalamocortical inputs, while a reduction of the fast excitatory activity (mediated by AMPA receptors) increases the probability to generate up-states in cortical layers 2/3 (Favero and Castro-Alamancos, 2013). Finally, the superficial cortical layer 2/3 is also known to receive long-range axons from other cortical areas that facilitate long-range synchronization (Yamashita et al., 2018). We have previously shown that SCI induces neuronal changes not only in the deprived HL cortex, but also in the adjacent, intact forelimb cortex (Humanes-Valera et al., 2017; Humanes-Valera et al., 2013; Yague et al., 2014). Therefore, changes in oscillatory synchronization in the sensory forelimb cortex may be transfer to hindlimb cortex through L2/3 corticocortical connections during spontaneous activity facilitating the up-state generation within the deprived cortical column. Despite of the mechanism used by the deprived cortex to generate spontaneous activity and to propagate the neuronal information across layers, the increase in L2/3 up-states may allow the deprived column to maintain its internal activity with possible implications in the processing of evoked sensory inputs as well as the reorganization of cortical areas after sensory deprivation.

Taking our results in the perspective of the long-term physiological effects that a SCI produces in the primary somatosensory cortex, it has been described how functional changes known as cortical reorganization can benefit functional recovery or induce pathophysiological consequences (i.e. neuropathic pain). There are two main factors involved in the development of CoRe: 1) structural changes of neuronal networks and connections linked to anatomical rewiring of axons and dendrites, and 2) functional changes linked to activity-dependent plasticity and/or homeostatic plasticity (Muret and Makin, 2020). Since our results were obtained in a narrow time window (from minutes to few hours after deprivation), the possibility of structural and/or anatomical changes is limited. On the contrary, we consider that the observed neuronal network alterations in a specific layer will depend on the importance of lacking the preferred connectivity (thalamocortical or corticocortical), the inhibitory neuronal composition and how the network integrates secondary/non-preferential and weak connections (as described in Muret and Makin, 2020). Then, immediate functional changes described in our results point to an initiation of homeostatic processes intended to compensate input deprivation by rebalancing excitation:inhibition as it has been described in other sensory systems (Keck et

al., 2013; Barnes et al., 2017; Teichert et al., 2017), which can be followed in the long-term by a process of activity-dependent plasticity. We found our results consistent with other deprivation models as amputation (Makin et al., 2013), in which has been described that the map remains stable, but the function is affected. Importantly, our work provides a new framework for a better understanding of CoRe after SCI by identifying a role for deprived supragranular layers in better integrating spontaneous corticocortical information to modify the excitability of the column, and for deprived infragranular layers in better integrating evoked-sensory inputs to preserve specific corticothalamic and cortico-subcortical networks. We postulate that the layer-specific neuronal changes observed immediately after sensory deprivation may guide the long-term alterations in neuronal excitability and plasticity linked to the rearrangements of somatosensory networks and the appearance of central sensory pathologies usually associated with SCI.

## MATERIALS AND METHODS

### Experimental approach

Experiments were performed on Wistar rats in accordance with the International Council for Laboratory Animal Science and the European Union 2010/63/EU guidelines. The experimental protocol was approved by the Ethical Committee for Animal Research at the Hospital Nacional de Parapléjicos (Toledo, Spain). Subjects were housed 2 per cages in standardized cages, with *ad libitum* access to food and water and maintained at 23 °C on a 12-hour light/dark cycle. A total of 24 male rats (range: 300-450 g; mean ± standard error of the mean, SEM: 400 ± 9.5 g) were used.

The general experimental approach (anaesthesia, surgery and peripheral stimulation) was similar to that used in our previous studies (Aguilar et al. 2010; Alonso-Calviño et al. 2016; Humanes-Valera et al. 2017; Humanes-Valera, Aguilar, and Foffani 2013). Briefly, animals were anaesthetised with an intraperitoneal injection of urethane (1.5 g/kg i.p.), placed in a stereotaxic frame (SR-6 Narishige Scientific Instruments, Tokyo, Japan) passively ventilated at 2 l $O_2$/min by a mask (Medical Supplies & Services, INT. LTD., England) and body temperature kept constant at 36.5ºC using a homeothermic blanket (Cibertec SL, Madrid, Spain). Then, lidocaine 2% was applied subcutaneously into the areas of the incision and thoracic laminectomy (at T9–T10 vertebra) was performed keeping the dura mater intact and protected until the moment of performing a complete transection of the spinal cord. Next, the skull was exposed, and a craniotomy was performed on the right hemisphere over the hindlimb representation of the primary somatosensory cortex (AP 0 to -3 mm; ML 1 to 4 mm) (Chapin and Lin, 1984; Paxinos and Watson, 2007) to allow lowering a vertical array for further record of neuronal activity. The stability of recordings was improved by drainage of the cisterna magna. The exact location of the probe was optimized by assessing the responses to tactile stimulation of the rat´s hindlimb with a cotton swab while listening to the recorded signal through a pair of loudspeakers.

### Electrophysiological recordings and peripheral stimulation

Extracellular recordings were obtained by a linear vertical probe of 32 iridium contacts with diameter 177 $\mu m^2$ spaced at 50 µm (impedance 1-4 MΩ at 1 kHz; NeuroNexus Technologies Inc., US). The array was slowly introduced (1-2 µm/s) through the craniotomy into the HLCx (Fiáth et al., 2019) and a ground electrode was placed in the parietal muscular tissue. The reference electrode was built in the vertical probe, 0.5 mm above the superficial recording site and outside the cortex (diameter 4200 $\mu m^2$). Recording protocol started ~40 min after the end of the electrode insertion to allow recovery of cortical tissue following time line in Figure 1A. Spontaneous activity was recorded during 10 min. Stimulation protocol (0.5 ms pulse duration at 0.5 Hz) was applied through bipolar needle electrodes located subcutaneously in the wrist of contralateral forelimb and hindlimb extremities. Two different intensities were applied: 1) low intensity (0.5 mA) to activate only a fraction of the available peripheral fibres, mainly low-threshold primary fibres running through the lemniscal pathway, from the dorsal column to the brainstem, and 2) high intensity (5 mA) to activate the maximum number of fibres including high-threshold primary fibres that synapse in the dorsal horns of the spinal cord including the spinothalamic tract (Lilja et al., 2006; Yague et al., 2011). After recordings of evoked and spontaneous activity in control conditions, complete transection of the spinal cord was performed using a spring scissors. Immediately after transection, pulses of 10 mA electrical stimulation were applied to the contralateral hindlimb to confirm that no physiological responses were evoked by stimuli delivered below the level of the lesion. Complete spinal cord transection was also visually confirmed under the surgical microscope by the total separation of the borders. Recordings were continuously

acquired during the transection to confirm the stability of the recordings. Approximately 20-30 min after the transection, the same protocol as before SCI was applied. Based on the absence of reflexes to forelimb stimuli, spontaneous whisker movements and corneal reflex, animals never received additional anaesthesia between the pre lesion protocol and the post lesion protocol. All recording data were converted into digital data at a 40 kHz sampling rate (16/24 rats) and 1kHz (8/24 rats), with 16–bit quantization by an OmniPlex System controlled by OmniPlex Server and PlexControl software (Plexon Inc, Texas, USA). All the 40 kHz signals were offline filtered (Spike2.v7, Cambridge Electronics Design, Cambridge, UK) into two signals: local field potentials (LFP, low-frequency band: up to 1kHz) and multiunit activity (MUA, high-frequency band: 0.3-3kHz).

### Data analysis: evoked responses and spontaneous activity

For laminar profile analysis, LFP evoked responses from each electrode were averaged across 100 stimuli (0.5 Hz) and measured as the maximum amplitude to negative peak (mV) in the local fast response in a time window corresponding to 5-60 ms or 5-30 ms following sensory stimulation of hindimb or forelimb, respectively. In order to quantify MUA, the filtered recordings were rectified (rMUA) and averaged across 100 stimuli to measure the total voltage resulting from the averaged area of responses (µV). The obtained value was then subtracted from the background voltage obtained 50 ms before stimulation. For layer analysis, LFP from electrodes within the same layer were obtained according to the depth: layer 2/3 (150-650 µm), layer 4 (700-1000 µm), layer 5 (1050-1450 µm) and layer 6 (1500-2000 µm; Fiáth et al., 2016). In the case of rMUA, neuronal signals obtained from individual channels within a layer were summed up to allow robust detection of the neuronal activity.

Onset latency of evoked-LFP and -rMUA was calculated for each layer by fitting the averaged response with an equation of the form of the Boltzmann charge–voltage function. This equation was solved for its 4th derivative giving a highly accurate measure of the response onset independent of the slope rise phase (Fedchyshyn and Wang 2007). Slopes were measured by using the next equation: $\frac{\Delta V}{t1-t2}$, where $\Delta V$ is the LFP amplitude, $t_1$ is the onset and $t_2$ is the time of the negative peak. For analysis of the spontaneous cortical activity, up-states within the slow-wave activity (SWA) were first analysed in periods of 5 minutes of spontaneous HLCx recordings for each subject to compare cortical state immediately before and between 10-30 minutes after SCI. Raw signals were down sampled to 500 Hz and then a Fast Fourier Transform (FFT) analysis was performed to confirm that the maximum peak frequency of the recordings was below 1 Hz. Frequency power ($mV^2$) was extracted for each electrode by summing power within same frequency band: SWA (0.1-1 Hz), delta (δ, 1-4 Hz), theta (θ, 4-8 Hz), alfa (α, 8-12 Hz), beta (β, 12-25 Hz), low gamma (Lγ, 25-50 Hz) and high gamma (Hγ, 50-80 Hz). LFP power obtained from individual electrodes within a layer was averaged to obtain a layer frequency power. Finally, the power of each frequency band was normalized to the total power of the LFP recording (0.1-80 Hz) to obtain the relative power of each band. Additionally, individual up-states were selected within periods of 60 seconds of LFP for each subject to obtain the onset in control and acute SCI using the same methodology than for the onset of evoked-LFP responses (Fedchyshyn and Wang 2007). To calculate the velocity of propagation, the electrode presenting the earliest onset was taken as reference, and the velocity rate calculated as the distance in the cortical depth as a function of time.

### Thalamocortical recordings and analysis

Simultaneous electrophysiological recordings from FLCx and HLCx (n = 7 rats) in response to peripheral forelimb stimulation were obtained by using two single tungsten electrodes located on infragranular layer 5 of both cortical regions under control conditions and after SCI. Note that this dataset was obtained simultaneously to the thalamic data previously published in Alonso-Calviño et al. (2016), but the cortical dataset has been for the first time analysed for the present work. Anaesthesia and stimulation protocol were the same than for experiments explained above. Extracellular recordings were obtained using tungsten electrodes (TM31C40KT, 4-MΩ impedance at 1 kHz or TM31A50KT, 5-MΩ impedance at 1 kHz; World Precision Instruments Inc., Sarasota FL, USA). All recordings were pre-amplified in the DC mode, low pass filtered (<3 kHz) and amplified using a modular system (Neurolog, Digitimer Ltd). Analogue signals were converted into digital data at a 20 kHz with 16–bit quantization via a CED power 1401 apparatus controlled by Spike2 software (v6, Cambridge Electronics Design, Cambridge, UK). The data was analysed using Spike2 software. Onset latency of cortical responses was obtained using the same method than for S1HL multielectrode recordings (Fedchyshyn and Wang 2007) and evoked cortical

responses to peripheral forelimb stimulation at 5 mA were used for this analysis.

### Histology

At the end of the experiments, animals were transcardially perfused with heparinised saline followed by 4% paraformaldehyde. Then the brain was removed and post-fixed in the same fixative solution for 24h at 4°C. After fixation, brain tissue was cryopreserved in a 30% sucrose solution until sank and coronal sections at 50 µm thick were obtained with a sliding microtome (Microm HM 450 V; Microm International GmbH, Walldorf, Germany). Following washing in 0.1 M phosphate buffer, sections were mounted in gelatin slides, air dried, processed for cresyl violet (Nissl) staining, dehydrated in xylene and coverslipped with DePeX (SEVA Electrophoresis GmbH, Heidelberg, Germany).

### Statistical analysis

Statistical analyses were performed using Statistica.Ink software (Statsoft Ibérica, Lisboa, Portugal). Shapiro-Wilk test was used to test normality distribution ($p > 0.05$). If normality was violated (non-gaussian distribution $p < 0.05$, rMUA responses), data were transformed to normal distribution by using square-root. Grubb´s test was used to identify and remove outliers (alpha = 0.05). Our main hypothesis (differences across layers) was first tested in our control data set (pre lesion) using one-way Analysis of Variance (ANOVA) with LAYER as independent factor. Dependent differences between pre- and post-injury among animals and layers were determined by two-way ANOVA, with LAYER as an independent factor and TIME as a repeated measures factor (two levels, PRE- and POST- lesion). When significant differences in analysis of variance where found, groups were further compared using Tukey´s *post hoc* test. For statistical analysis of the dual recording site from intact and deafferented cortices (Figure 5), we used two-tailed paired t-test with a *Bonferroni's* correction for multiple comparisons ($p < 0.025$). The threshold for statistical significance was $p < 0.05$ throughout. Group measurements are expressed as mean ± standard error of the mean (SEM). Results from statistical analysis are summarized in Table 1-3 of supplementary material.

## ACKNOWLEGMENTS

We thank Dr. Casto Rivadulla for helpful comments on the manuscript. This work was supported by Ministerio de Economía y Competitividad and Ministerio de Ciencia, Innovación y Universidades, Spanish Government, BFU2016-80665-P and PID2019-105020GB to J.A., SAF2016-80647-R to A.O., both co-funded by FEDER; European Union's Horizon 2020 research and innovation programme under the Marie Sklodowska-Curie grant agreement Nº 794926 to J.M.R. and predoctoral fellowship FPI-MICINN from the Ministerio de Ciencia, Innovación y Universidades, Spanish Government BES2017-082029 to M.Z.

## AUTHOR CONTRIBUTIONS

Conceptualization, J.A.; Methodology, M.Z., J.M.R., C.M-Q., E.A-C., E.F-L., J.A.; Investigation, M.Z., J.M.R., C.M-Q., E.A-C., E.F-L.; Original Draft, J.M.R., M.Z., J.A.; Writing–Review & Editing, M.Z., C.M-Q., J.M.R., E.A-C., E.F-L., A.O., J.A.; Visualization, M.Z., J.M.R., J.A.; Funding Acquisition, J.M.R. A.O., J.A.

## DECLARATION OF INTERESTS

The authors declare no competing interests.

## REFERENCES

Aguilar J, Humanes-Valera D, Alonso-Calviño E, Yague JG, Moxon KA, Oliviero A, Foffani G. (2010) Spinal cord injury immediately changes the state of the brain. J Neurosci. 30,7528-37.

Alonso-Calviño E, Martínez-Camero I, Fernández-López E, Humanes-Valera D, Foffani G, Aguilar J. (2016). Increased responses in the somatosensory thalamus immediately after spinal cord injury. Neurobiol Dis.87,39-49.

Barnes SJ, Franzoni E, Jacobsen RI, Erdelyi F, Szabo G, Clopath C, Keller GB, Keck T. (2017). Deprivation-Induced Homeostatic Spine Scaling In Vivo Is Localized to Dendritic Branches that Have Undergone Recent Spine Loss. Neuron.96,871-882.

Bayraktar OA, et al. (2020) Astrocyte layers in the mammalian cerebral cortex revealed by a single-cell in situ transcriptomic map. Nat Neurosci. 23,500-509

Bola Ł, Zimmermann M, Mostowski P, Jednoróg K, Marchewka A, Rutkowski P, Szwed M. (2017). Task-specific reorganization of the auditory cortex in deaf humans. PNAS U S A. 114,E600-E609.

Buzsáki G, Anastassiou CA, Koch C. (2012). The origin of extracellular fields and currents--EEG, ECoG, LFP and spikes.Nat Rev Neurosci. 13,407-20

Cardin JA, Carlén M, Meletis K, Knoblich U, Zhang F, Deisseroth K, Tsai LH, Moore CI. (2009). Driving fast-spiking cells induces gamma rhythm and controls sensory responses. Nature. 459,663-7.

Castro-Alamancos MA. (2009). Cortical up and activated states: implications for sensory information processing. Neuroscientist. 15,625-34.

Chand P, Jain N. (2015). Intracortical and Thalamocortical Connections of the Hand and Face Representations in Somatosensory Area 3b of Macaque Monkeys and Effects of Chronic Spinal Cord Injuries. J Neurosci. 2015. 35(39):13475-86.

Chapin JK, Lin CS. (1984). Mapping the body representation in the SI cortex of anesthetized and awake rats. J Comp Neurol. 229,199-213.

Chauvette S, Volgushev M, Timofeev I. (2010). Origin of active states in local neocortical networks during slow sleep oscillation. Cereb Cortex. 20,2660-74.

Compte A, Sanchez-Vives MV, McCormick DA, Wang XJ. (2003). Cellular and network mechanisms of slow oscillatory activity (<1 Hz) and wave propagations in a cortical network model. J Neurophysiol. 89,2707-25.

Curt A, Bruehlmeier M, Leenders KL, Roelcke U, Dietz V. (2002). Differential effect of spinal cord injury and functional impairment on human brain activation. J Neurotrauma. 19,43-51.

David F, Schmiedt JT, Taylor HL, Orban G, Di Giovanni G, Uebele VN, Renger JJ, Lambert RC, Leresche N, Crunelli V. (2013). Essential thalamic contribution to slow waves of natural sleep. J Neurosci. 33,19599-610.

De Pasquale R, Sherman SM. (2011) Synaptic properties of corticocortical connections between the primary and secondary visual cortical areas in the mouse. J Neurosci. 31,16494-506.

Derdikman D, Yu C, Haidarliu S, Bagdasarian K, Arieli A, Ahissar E. (2006). Layer-specific touch-dependent facilitation and depression in the somatosensory cortex during active whisking. J Neurosci. 26,9538-47.

Dutta A, Kambi N, Raghunathan P, Khushu S, Jain N. (2014). Large-scale reorganization of the somatosensory cortex of adult macaque monkeys revealed by fMRI. Brain Struct Funct. 219,1305-20.

Endo T, Spenger C, Tominaga T, Brené S, Olson L. (2007). Cortical sensory map rearrangement after spinal cord injury: fMRI responses linked to Nogo signalling. Brain. 130,2951-61.

Favero M, Castro-Alamancos MA. (2013). Synaptic cooperativity regulates persistent network activity in neocortex. J Neurosci. 33,3151-63.

Fedchyshyn MJ, Wang LY. (2007). Activity-dependent changes in temporal components of neurotransmission at the juvenile mouse calyx of Held synapse. J Physiol. 581,581-602. doi: 10.1113/jphysiol.2007.129833.

Fernández-López E, Alonso-Calviño E, Humanes-Valera D, Foffani G, Aguilar J. (2019) Slow-wave activity homeostasis in the somatosensory cortex after spinal cord injury. Exp Neurol. 322,113035.

Fiáth R, Kerekes BP, Wittner L, Tóth K, Beregszászi P, Horváth D, Ulbert I. (2016). Laminar analysis of the slow wave activity in the somatosensory cortex of anesthetized rats. Eur J Neurosci. 44,1935-51.

Fiáth R, Márton AL, Mátyás F, Pinke D, Márton G, Tóth K, Ulbert I. (2019). Slow insertion of silicon probes improves the quality of acute neuronal recordings. Sci Rep. 9,111.

Flor H, Elbert T, Knecht S, Wienbruch C, Pantev C, Birbaumer N, Larbig W, Taub E. (1995). Phantom-limb pain as a perceptual correlate of cortical reorganization following arm amputation. Nature. 375(6531):482-4.

Francis JT, Xu S, Chapin JK. (2008). Proprioceptive and cutaneous representations in the rat ventral posterolateral thalamus.J Neurophysiol. 99,2291-304

Freund P, Weiskopf N, Ashburner J, Wolf K, Sutter R, Altmann DR, Friston K, Thompson A, Curt A. (2013). MRI investigation of the sensorimotor cortex and the corticospinal tract after acute spinal cord injury: a prospective longitudinal study. Lancet Neurol. 12,873-881.

Ghosh A, Haiss F, Sydekum E, Schneider R, Gullo M, Wyss MT, Mueggler T, Baltes C, Rudin M, Weber B, Schwab ME. (2010). Rewiring of hindlimb corticospinal neurons after spinal cord injury. Nat Neurosci. 13,97-104.

Green JB, Sora E, Bialy Y, Ricamato A, Thatcher RW. (1998). Cortical sensorimotor reorganization after spinal cord injury: an electroencephalographic study. Neurology. 50,1115-21.

Griffen TC, Haley MS, Fontanini A, Maffei A. (2017). Rapid plasticity of visually evoked responses

in rat monocular visual cortex. PLoS One. 12,e0184618.

Gruber T, Tsivilis D, Montaldi D, Müller MM. (2004). Induced gamma band responses: an early marker of memory encoding and retrieval. Neuroreport. 15,1837-41.

Gustin SM, Wrigley PJ, Siddall PJ, Henderson LA. (2010). Brain anatomy changes associated with persistent neuropathic pain following spinal cord injury. Cereb Cortex. 20,1409-19.

Han Y, Li N, Zeiler SR, Pelled G. (2013). Peripheral nerve injury induces immediate increases in layer v neuronal activity. Neurorehabil Neural Repair. 27,664-72.

He HY, Hodos W, Quinlan EM. (2006). Visual deprivation reactivates rapid ocular dominance plasticity in adult visual cortexJ Neurosci. 26,2951-5

Humanes-Valera D, Aguilar J, Foffani G. (2013). Reorganization of the intact somatosensory cortex immediately after spinal cord injury. PLoS One. 8,e69655.

Humanes-Valera D, Foffani G, Alonso-Calviño E, Fernández-López E, Aguilar J. (2017). Dual Cortical Plasticity After Spinal Cord Injury. Cereb Cortex. 27,2926-2940.

Jain N, Florence SL, Kaas JH. (1998). Reorganization of Somatosensory Cortex After Nerve and Spinal Cord Injury. News Physiol Sci. 13,143-149.

Jain N, Florence SL, Qi HX, Kaas JH. (2000). Growth of new brainstem connections in adult monkeys with massive sensory loss. Proc Natl Acad Sci U S A. 97,5546-50.

Jain N, Qi HX, Collins CE, Kaas JH. (2008). Large-scale reorganization in the somatosensory cortex and thalamus after sensory loss in macaque monkeys. J Neurosci. 28,11042-60.

Jutzeler CR, Curt A, Kramer JL. (2015). Relationship between chronic pain and brain reorganization after deafferentation: A systematic review of functional MRI findings. Neuroimage Clin. 9,599-606.

Jutzeler CR, Streijger F, Aguilar J, Shortt K, Manouchehri N, Okon E, Hupp M, Curt A, Kwon BK, Kramer JLK. (2018). Sensorimotor plasticity after spinal cord injury: a longitudinal and translational study. Ann Clin Transl Neurol. 6,68-82.

Kao T, Shumsky JS, Murray M, Moxon KA. (2009). Exercise induces cortical plasticity after neonatal spinal cord injury in the rat. J Neurosci. 29,7549-57.

Keck T, Keller GB, Jacobsen RI, Eysel UT, Bonhoeffer T, Hübener M. (2013). Synaptic scaling and homeostatic plasticity in the mouse visual cortex in vivo. Neuron. 80,327-34.

Kriegeskorte N, Simmons WK, Bellgowan PS, Baker CI. (2009). Circular analysis in systems neuroscience: the dangers of double dipping. Nat Neurosci. 12(5):535-40.

Kuki T, Fujihara K, Miwa H, Tamamaki N, Yanagawa Y, Mushiake H. (2015). Contribution of parvalbumin and somatostatin-expressing GABAergic neurons to slow oscillations and the balance in beta-gamma oscillations across cortical layers. Front Neural Circuits. 9,6.

Liang L, Mendell LM. (2013). Bilateral transient changes in thalamic nucleus ventroposterior lateralis after thoracic hemisection in the rat. J Neurophysiol. 110,942-51.

Lilja J, Endo T, Hofstetter C, Westman E, Young J, Olson L, Spenger C. (2006). Blood oxygenation level-dependent visualization of synaptic relay stations of sensory pathways along the neuroaxis in response to graded sensory stimulation of a limb. J Neurosci. 26,6330-6.

Makin TR, Scholz J, Filippini N, Henderson Slater D, Tracey I, Johansen-Berg H. (2013). Phantom pain is associated with preserved structure and function in the former hand area. Nat Commun. 4,1570.

Makin TR, Scholz J, Henderson Slater D, Johansen-Berg H, Tracey I. (2015). Reassessing cortical reorganization in the primary sensorimotor cortex following arm amputation. Brain. 138(Pt 8):2140-6.

Makin TR, Orban de Xivry JJ. (2019). Ten common statistical mistakes to watch out for when writing or reviewing a manuscript. Elife. 8:e48175.

Minlebaev M, Colonnese M, Tsintsadze T, Sirota A, Khazipov R. (2011). Early γ oscillations synchronize developing thalamus and cortex. Science. 334,226-9.

Morales-Botello ML, Aguilar J, Foffani G. (2012). Imaging the spatio-temporal dynamics of supragranular activity in the rat somatosensory cortex in response to stimulation of the paws. PLoS One. 7,e40174.

Moxon KA, Hale LL, Aguilar J, Foffani G. (2008). Responses of infragranular neurons in the rat primary somatosensory cortex to forepaw and hindpaw tactile stimuli. Neuroscience. 156,1083-92.

Moxon KA, Oliviero A, Aguilar J, Foffani G. (2014). Cortical reorganization after spinal cord injury: always for good?. Neuroscience 283, 78-94.

Muret D, Makin TR. (2020) The homeostatic homunculus: rethinking deprivation-triggered reorganisation. Curr Opin Neurobiol. 67,115-122.

Ortmann M, Müller N, Schlee W, Weisz N. (2011). Rapid increases of gamma power in the auditory cortex following noise trauma in humans. Eur J Neurosci. 33,568-75.

Paxinos G, Watson C. (2007). The rat brain in stereotaxic coordinates (6th Ed.). Amsterdam: Academic Press. ISBN: 9780123741219.

Peyron R, Schneider F, Faillenot I, Convers P, Barral FG, Garcia-Larrea L, Laurent B. (2004). An fMRI study of cortical representation of mechanical allodynia in patients with neuropathic pain. Neurology. 63,1838-46.

Puig MV, Ushimaru M, Kawaguchi Y. (2008). Two distinct activity patterns of fast-spiking interneurons during neocortical UP states. Proc Natl Acad Sci U S A. 105,8428-33.

Rigas P, Castro-Alamancos MA. (2009). Impact of persistent cortical activity (up States) on intracortical and thalamocortical synaptic inputs. J Neurophysiol. 102,119-31.

Rossignol S, Frigon A. (2011). Recovery of locomotion after spinal cord injury: some facts and mechanisms. Annu Rev Neurosci. 34,413-40.

Sakata S, Harris KD. (2009). Laminar structure of spontaneous and sensory-evoked population activity in auditory cortex. Neuron. 64,404-18.

Sanchez-Vives MV, McCormick DA. (2000). Cellular and network mechanisms of rhythmic recurrent activity in neocortex. Nat Neurosci. 3,1027-34.

Schoffelen JM, Poort J, Oostenveld R, Fries P. (2011). Selective movement preparation is subserved by selective increases in corticomuscular gamma-band coherence. J Neurosci. 31,6750-8.

Schroeder CE, Mehta AD, Givre SJ. (1998). A spatiotemporal profile of visual system activation revealed by current source density analysis in the awake macaque. Cereb Cortex. 8,575-92.

Schubert D, Kötter R, Staiger JF. (2007). Mapping functional connectivity in barrel-related columns reveals layer- and cell type-specific microcircuits. Brain Struct Funct. 212,107-19.

Siddall PJ, Loeser JD. (2001). Pain following spinal cord injury. Spinal Cord. 39,63-73.

Siddall PJ, McClelland JM, Rutkowski SB, Cousins MJ. (2003). A longitudinal study of the prevalence and characteristics of pain in the first 5 years following spinal cord injury. Pain. 103,249-57.

Steriade M, McCormick DA, Sejnowski TJ. (1993). Thalamocortical oscillations in the sleeping and aroused brain. Science. 262,679-85.

Sydekum E, Ghosh A, Gullo M, Baltes C, Schwab M, Rudin M. (2014). Rapid functional reorganization of the forelimb cortical representation after thoracic spinal cord injury in adult rats. Neuroimage. 87,72-9.

Tan LL, Oswald MJ, Heinl C, Retana Romero OA, Kaushalya SK, Monyer H, Kuner R. (2019). Gamma oscillations in somatosensory cortex recruit prefrontal and descending serotonergic pathways in aversion and nociception. Nat Commun. 10,983.

Teichert M, Liebmann L, Hübner CA, Bolz J. (2017). Homeostatic plasticity and synaptic scaling in the adult mouse auditory cortex. Sci Rep. 7,17423.

Timofeev I, Grenier F, Bazhenov M, Sejnowski TJ, Steriade M. (2000). Origin of slow cortical oscillations in deafferented cortical slabs. Cereb Cortex. 10,1185-99.

Veit J, Hakim R, Jadi MP, Sejnowski TJ, Adesnik H. (2017). Cortical gamma band synchronization through somatostatin interneurons. Nat Neurosci. 20,951-959.

Welle CG, Contreras D. (2006). Sensory-driven and spontaneous gamma oscillations engage distinct cortical circuitry. J Neurophysiol. 115,1821-35.

Wester JC, Contreras D. (2012). Columnar interactions determine horizontal propagation of recurrent network activity in neocortex. J Neurosci. 32,5454-71.

Wester JC, Contreras D. (2013). Differential modulation of spontaneous and evoked thalamocortical network activity by acetylcholine level in vitro. J Neurosci. 33,17951-66.

Wilent WB, Contreras D. (2004). Synaptic responses to whisker deflections in rat barrel cortex as a function of cortical layer and stimulus intensity. J Neurosci. 24,3985-98.

Wrigley PJ, Press SR, Gustin SM, Macefield VG, Gandevia SC, Cousins MJ, Middleton JW, Henderson LA, Siddall PJ. (2009) Neuropathic pain and primary somatosensory cortex reorganization following spinal cord injury. Pain. 141,52-9.

Wrigley PJ, Siddall PJ, Gustin SM. (2018). New evidence for preserved somatosensory pathways in complete spinal cord injury: A fMRI study. Hum Brain Mapp. 39(1):588-598.

Yague JG, Foffani G, Aguilar J. (2011). Cortical hyperexcitability in response to preserved spinothalamic inputs immediately after spinal cord hemisection. Exp Neurol. 227,252-63.

Yagüe JG, Humanes-Valera D, Aguilar J, Foffani G. (2014). Functional reorganization of the forepaw cortical representation immediately after thoracic spinal cord hemisection in rats. Exp Neurol. 257,19-24.

Yamashita T, Vavladeli A, Pala A, Galan K, Crochet S, Petersen SSA, Petersen CCH. (2018) Diverse Long-Range Axonal Projections of Excitatory Layer 2/3 Neurons in Mouse Barrel Cortex. Front Neuroanat. 12,33.

FIGURE 1

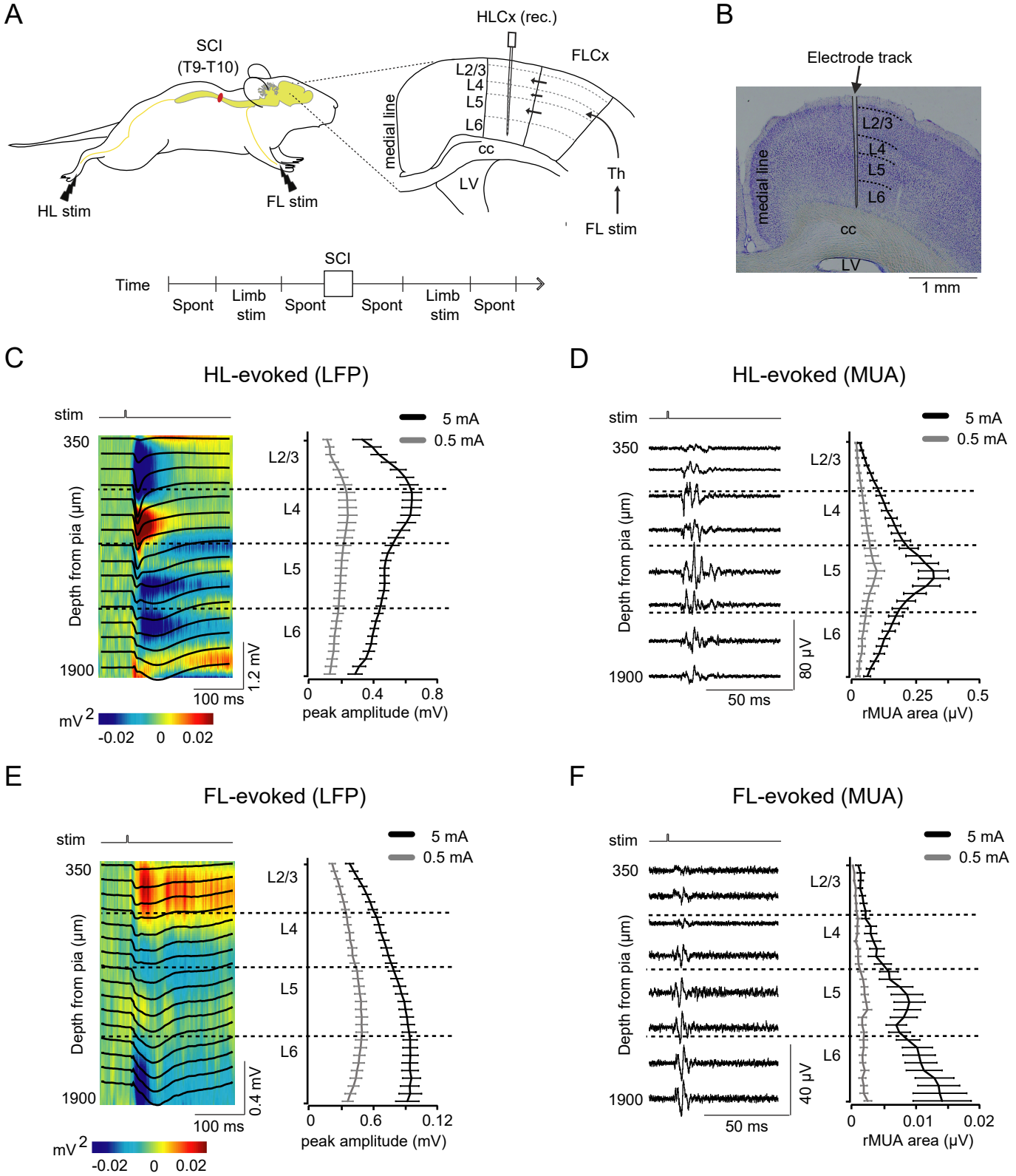


*Figure 1: Experimental approach and laminar characterization of evoked sensory responses in hindlimb cortex.* (A) Schematic illustration of the experimental protocol. Extracellular recordings were obtained using a multielectrode probe inserted in the hindlimb representation of the primary somatosensory cortex (HLCx) from anaesthetized rats. Complete transection of the spinal cord was performed at thoracic level (SCI, T9-T10). Spontaneous activity (Spont) and evoked responses to electrical stimulation at high (5 mA) and low (0.5 mA) intensity delivered to the contralateral hindlimb (HL stim) and forelimb (FL stim) were recorded following the described timeline in control conditions and immediately after SCI. In the cortical representation, black arrows indicate corticocortical connections and thalamic inputs into FL cortex in response to forepaw stimulation (FL stim). Cortical layers were designated as L2/3, L4, L5 and L6. Dashed black lines indicate boundaries of cortical layers. Corpus callosum, cc; Lateral ventricle, LV; Thalamus, Th. (B) Nissl-stained coronal section of a representative rat showing an electrode track in HL cortex. (C) Left: representative sensory evoked-LFP across HL cortical layers in response to a 5 mA electrical stimulation of the contralateral hindlimb (HL). Recordings obtained on every 100 µm are shown on top of the current source density (CSD) map from the same recordings. Right: averaged evoked-LFP amplitudes as a function of cortical depth in response to low (0.5 mA, grey) and high (5 mA, black) sensory stimulation. (D) Left: High-filtered LFP traces from the same recordings in C showing evoked-MUA signal. Right: Averaged area of rMUA from the same population in C. (E) Left: Representative traces of evoked-LFP overlapped on the CSD map in response to 5 mA forelimb stimulation from the same animal as C-D. Note that in this case current sinks are stronger in L2/3 and L5. Right: averaged evoked-LFP amplitudes as a function of cortical depth in response to low (0.5 mA, grey) and high (5 mA, black) sensory stimulation. (F) Left: High-filtered LFP traces from the same recordings in E showing evoked-MUA signal. Right: Averaged area of rMUA from the same population in E. Dashed black lines indicate borders between layers. Data are mean ± sem (n= 24 rats). See also - Supplemental Table 1.

FIGURE 2

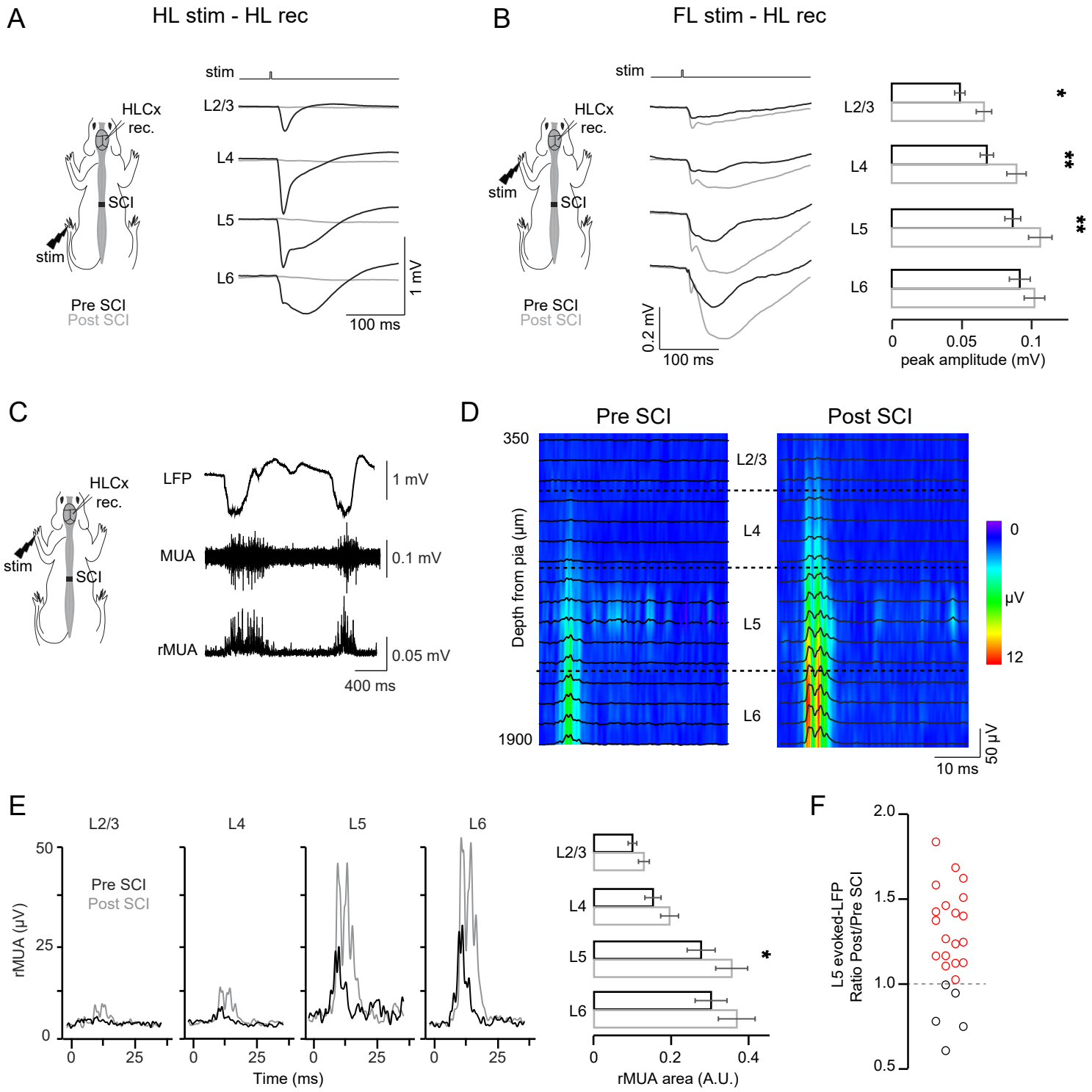


*Figure 2: Spinal cord injury induces functional changes in the S1 deprived cortex in a layer-dependent manner.* (A) Schematic showing the place of cortical recordings (HLCx rec) and hindlimb stimulation (HL stim). Examples of evoked-LFP averaged across electrode sites within each layer recorded in HLCx in response to HL stim (5 mA) in control (Pre SCI, black) and after SCI (Post SCI, grey). Note that complete spinal cord transection was confirmed by absence of evoked-LFP in HLCx. (B) Left, schematic showing HLCx rec and forelimb stimulation (FL stim) used for B-F. Examples of averaged evoked-LFP recorded in HLCx in response to FL stim (5 mA) in control and after SCI. Bars graph shows the population average of the evoked-LFP amplitude. (C) Original traces of LFP (top), multi-unit activity (MUA, middle) and rectified MUA (rMUA, bottom) in HLCx obtained following FL stim (5 mA). (D) Representative laminar profile of evoked-rMUA (black traces) overlapped to a colour map showing averaged HLCx responses to FL stim at 5 mA pre- and post-SCI. (E) Averaged evoked-rMUA across electrodes within distinct layers pre- and post-SCI and population averaged rMUA area. (F) Scattering plot showing ratio of layer 5 recordings calculated from evoked-LFP post-/pre-SCI. Dotted line represents ratio = 1. Dots represent individual experiments (red: ratio < 1, black: ratio > 1. Example traces in A-E are representative from the same animal. Data are mean ± sem (n = 24 rats for evoked-LFP and 16 rats for evoked-rMUA). * $p < 0.05$, ** $p < 0.01$. See also – Supplemental Table 2 and Supplemental Figure 1.

FIGURE 3

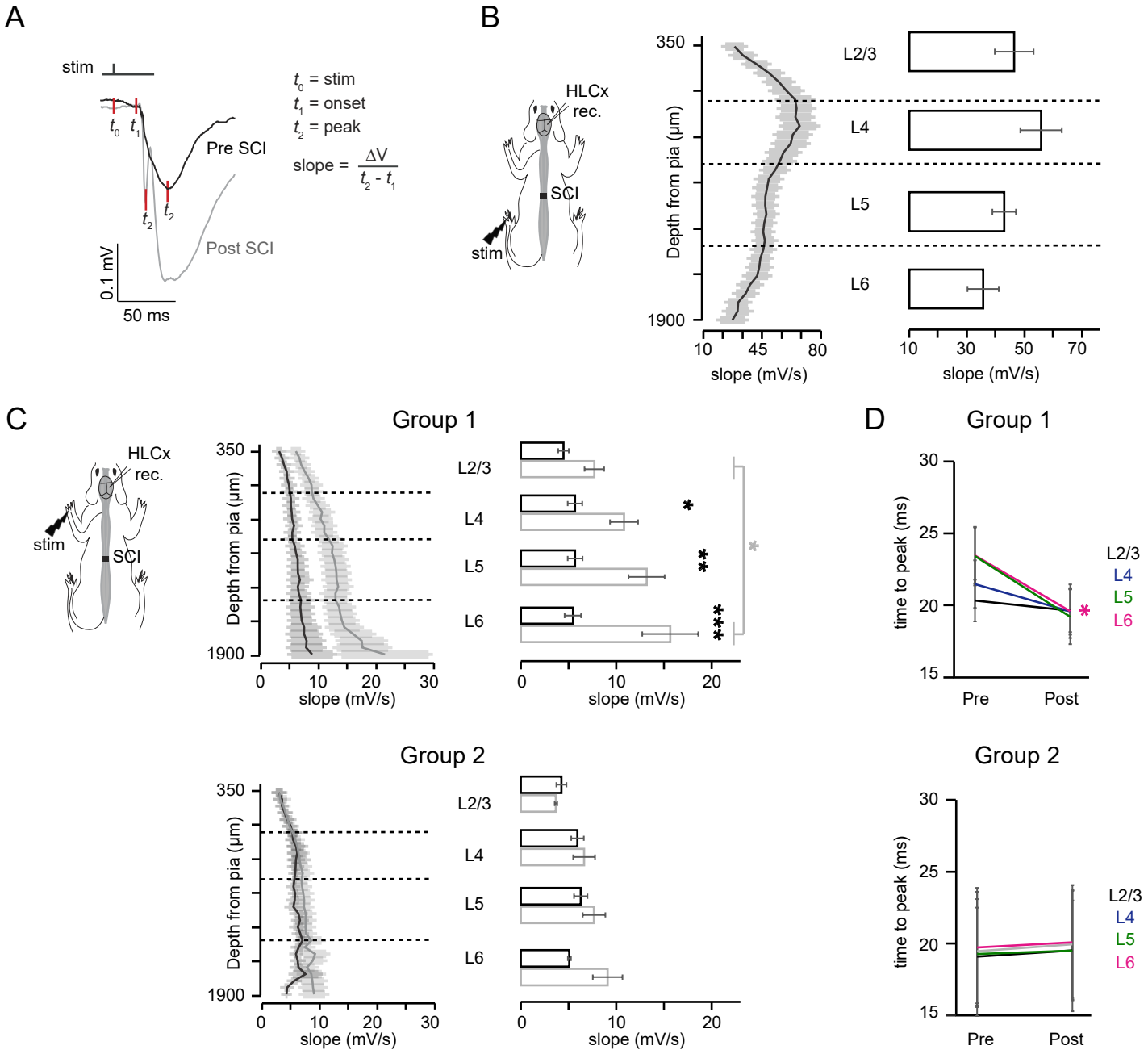


*Figure 3: Laminar profile properties of evoked responses following SCI.* (A) Original traces of averaged evoked-LFP in control condition (black) and after SCI (grey) illustrating the parameters used for slope analysis. (B) Scheme of an animal showing the place of cortical recordings (HLCx rec) and hindlimb stimulation (HL stim). Averaged slope of evoked-LFP from HLCx in response to HL stim at 5 mA in control. Bar graph shows the averaged slope values across electrodes within the same layer (n = 5 rats). (C) Averaged slope of evoked-LFP from HLCx in response to FL stim at 5 mA pre- and post-SCI for animals within Group 1 (top) and Group 2 (bottom). Bar graph shows the average slope values across electrodes within the same layer (n = 19, group 1, and n = 5, group 2). (F) Time-to-peak of the evoked-LFP responses before and after SCI from t0 to t2. Data are mean ± sem. * $p < 0.05$, ** $p < 0.01$, *** $p < 0.001$.

FIGURE 4

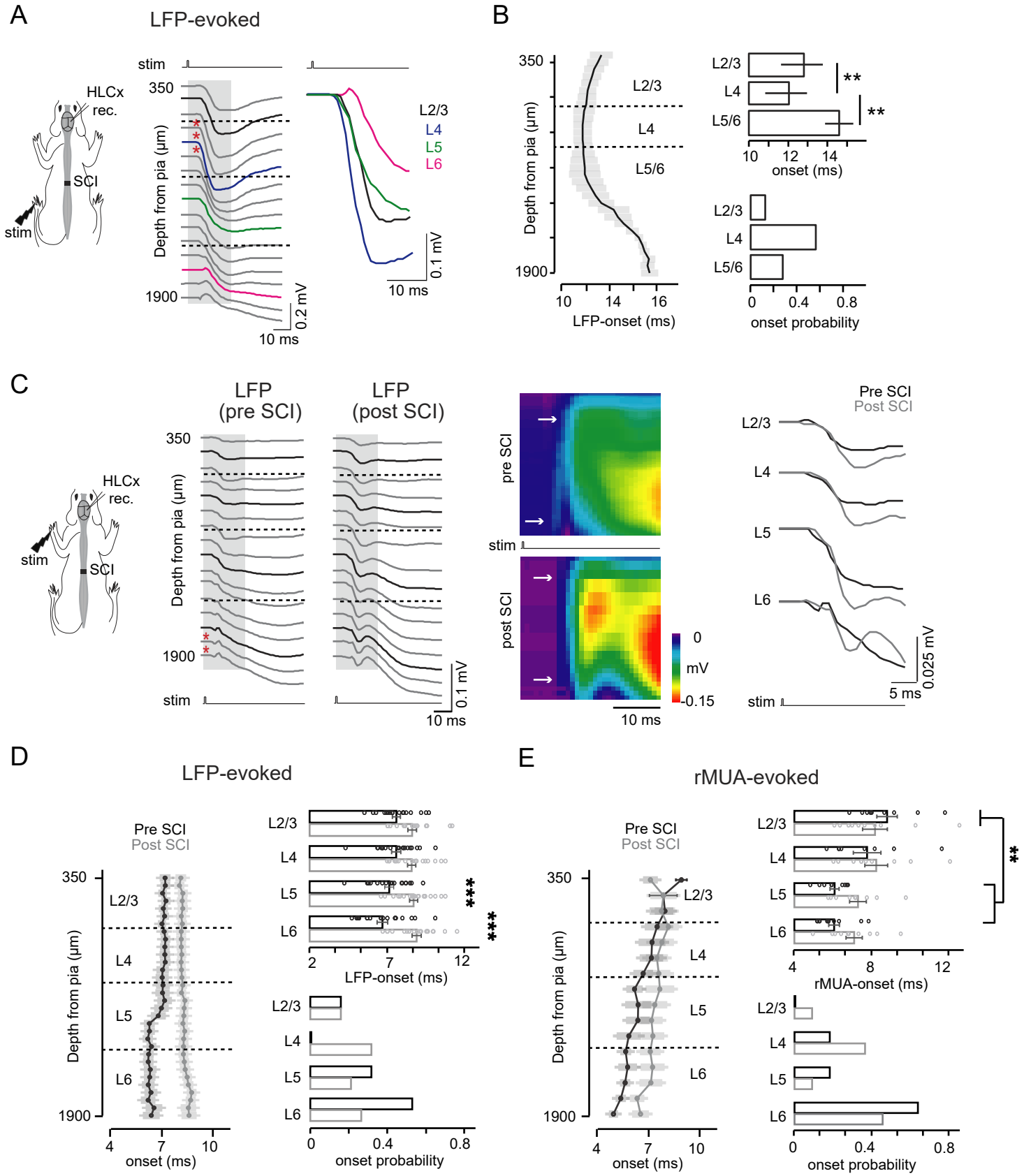


*Figure 4: Deprived infragranular layers exhibits delayed evoked-onset responses.* (A) Left: onset profile of evoked-LFP in HLCx in response to hindlimb stimulation (HL stim) before SCI. Red markers indicate electrodes in which evoked response started. Grey area indicates the period of response onset taken to highlighted LFP traces (in black) in the right. (B) Latency-onset averaged profile to hindlimb stimulation (5 mA) at left. Note the onset in the thalamorecipient granular layers (L4). Right top: bar graph of the evoked-LFP onset responses. Right bottom: normalized histogram of the evoked-LFP onset probability from. Data used in B contain a representative population (n = 5). (C) Left: onset profiles from the same animal pre- and post-SCI showing averaged evoked-LFP in HLCx in response to forelimb stimulation represented as in A. Middle: colour maps from the same traces that at left laminar profile. White arrows indicate the onset response in L2/3 and L6. Right: Highlighted LFP traces represented as black traces in C. In D-E, latency-onset of the laminar profile (at left) and averaged across layers (at right) by forelimb stimulation (5 mA) is represented for Group 1 for evoked-LFP (D) and -rMUA (E) analysis. Response latency-onset was quantified as the response beginning time (top bar graph) and normalized onset probability (bottom bar graph). Dots represent individual experiments. Data are mean ± sem (n = 19 rats for evoked-LFP and n = 13 rats for evoked-rMUA). Statistical significance is shown by asterisks for SCI effect and lines with asterisks for layer effect in each condition, ** $p < 0.01$, *** $p < 0.001$. See also – Supplemental Figure 1.

FIGURE 5

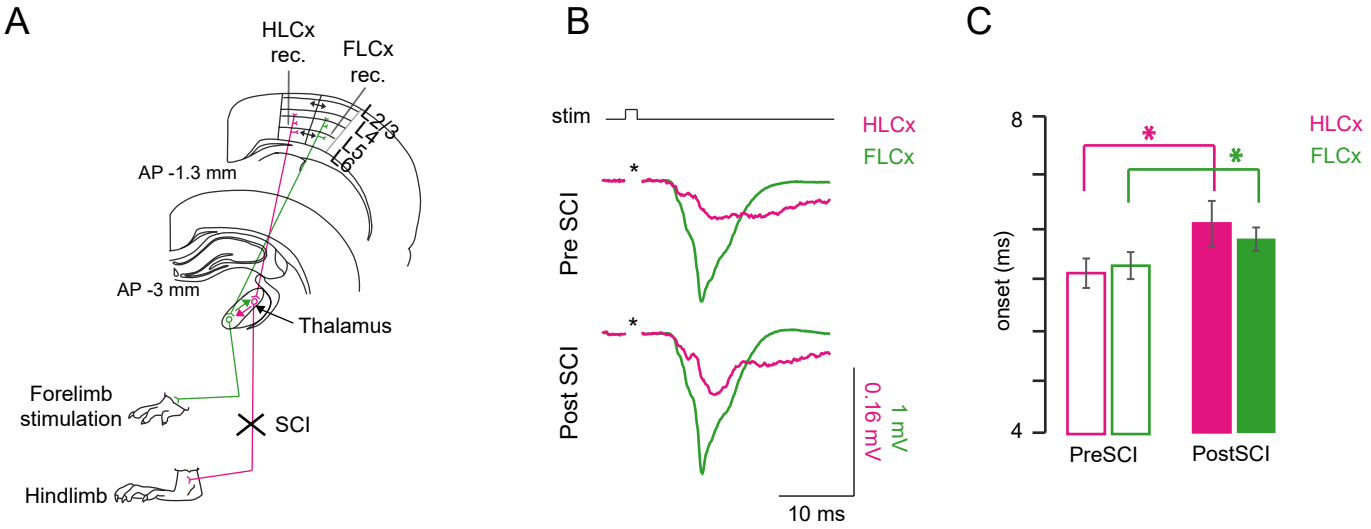


*Figure 5: Thalamocortical responses in HL cortex are delayed after SCI.* (A) Scheme showing the thalamocortical pathways activated after forelimb and hindlimb stimulation. Extracellular recordings were simultaneously obtained from L5 of HLCx and FLCx while forelimb stimulation at 5 mA was applied. Colored arrows in thalamic nucleus represent the collaterals allowing reciprocal activation of neighbor regions. (B) Original field potential traces obtained from simultaneous recordings from HLCx (magenta traces) and FLCx (green traces) before and after SCI. (C) Averaged bar graphs displaying onset latencies of evoked responses in HLCx and FLCx. Data are mean ± sem (n = 7 rats). * $p < 0.025$.

FIGURE 6

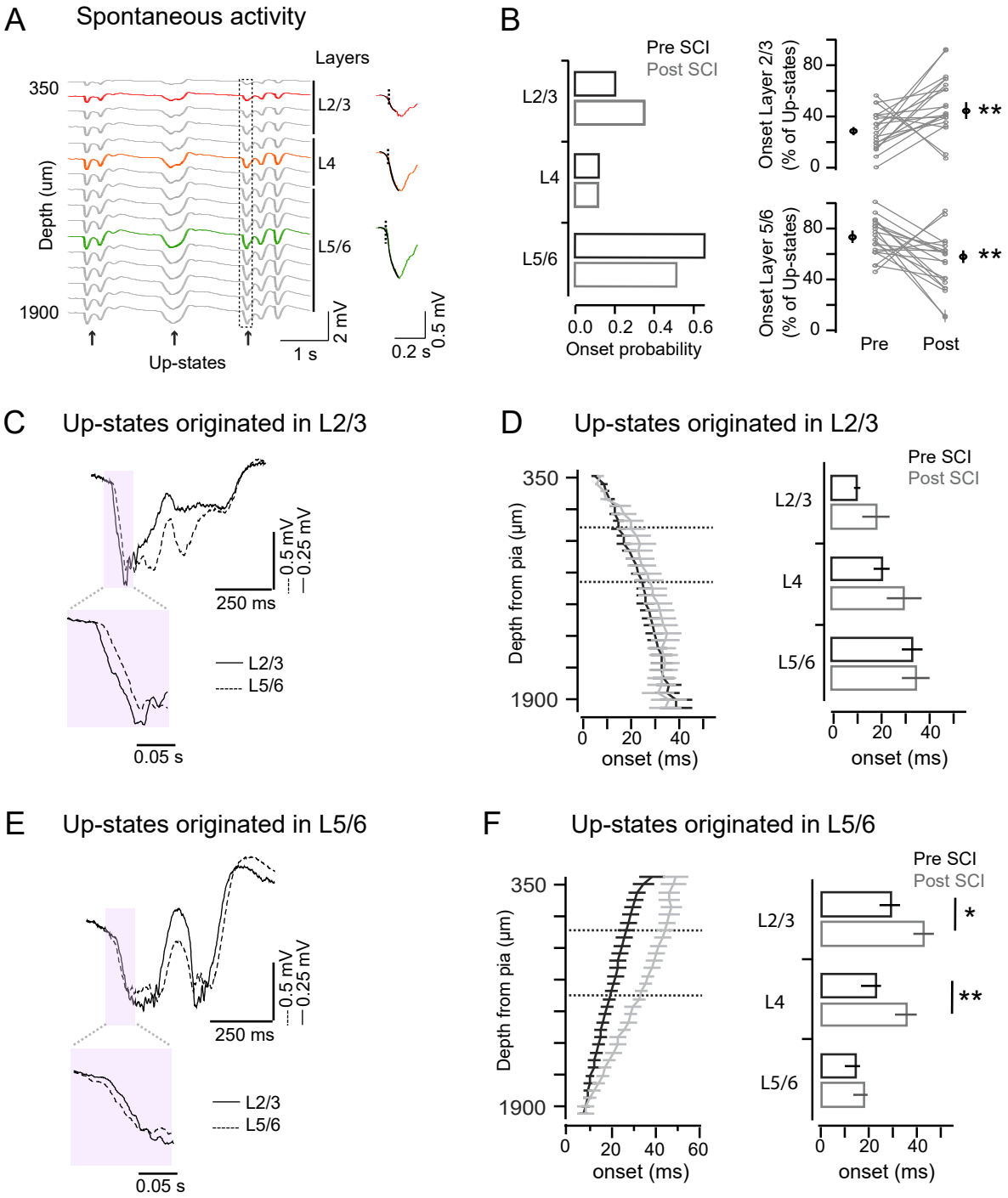


*Figure 6: Onset and propagation of spontaneous up-states is altered after SCI.* (A) Example SWA across electrodes (left) showing insets of the sigmoid fitting used to calculate the onset latency (right). Colours indicate distinct layers. (B) Left: Histogram of onset probability across layers of spontaneous up-states pre- and post-SCI. Right: Percentage of up-states with origin in layer 2/3 or layer 5/6 pre- and post-SCI. Lines represent each individual. Black dots are mean +- sem. (C) Representative example of spontaneous up-state with origin in layer 2/3 (black line) and delayed L5/6 (dotted line). Insets are magnification of magenta areas. (D) Laminar profile and averaged onset latencies of up-states originating in layer 2/3. (E) Representative example of spontaneous up-state with origin in layer 5/6 (dotted line) and delayed L2/3 (black line). (F) Laminar profile and averaged onset latencies of up-states originating in layer 5/6. Data are mean +- sem (n = 19 rats). * $p < 0.05$, ** $p < 0.01$.

FIGURE 7

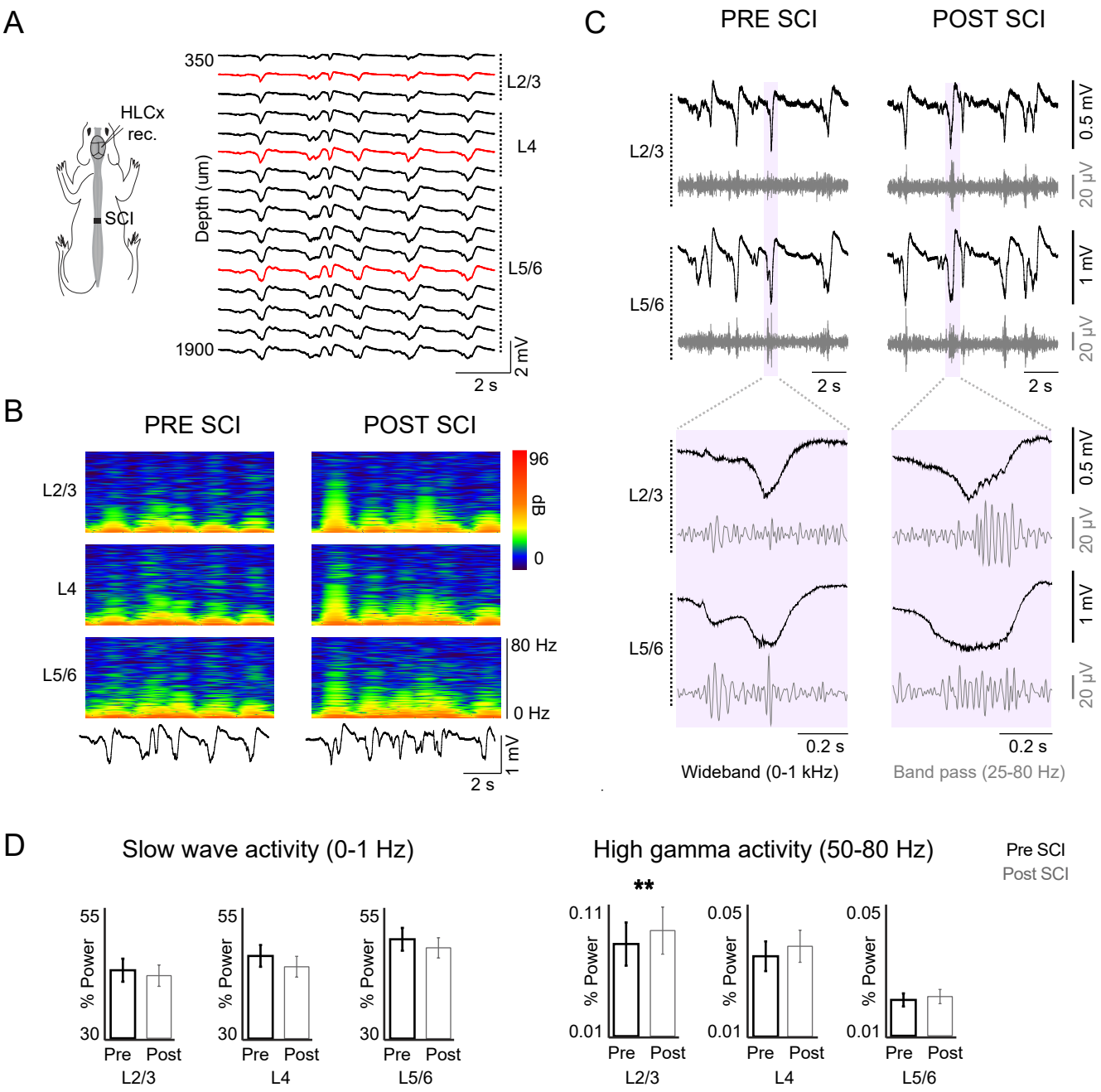


*Figure 7: SCI increases high-gamma frequency oscillations in supragranular layers.* (A) Example of spontaneous SWA profile recorded from HLCx in control conditions. Red traces represent selected electrodes within each cortical layer used for B-C. (B) Colour plots showing spontaneous SWA spectrogram in L2/3, L4 and L5/6 pre- and post-SCI. (C) Wideband signal (black) and gamma-filtered (25-80 Hz, grey) traces of SWA from L2/3 and L5/6 with expanded traces of the indicated time window. (D) SWA and gamma relative power from distinct layers before and after SCI. Data are mean ± sem (n = 19 rats). ** $p < 0.01$. See algo – Supplemental Table 3.

# SUPPLEMENTARY FIGURE 1

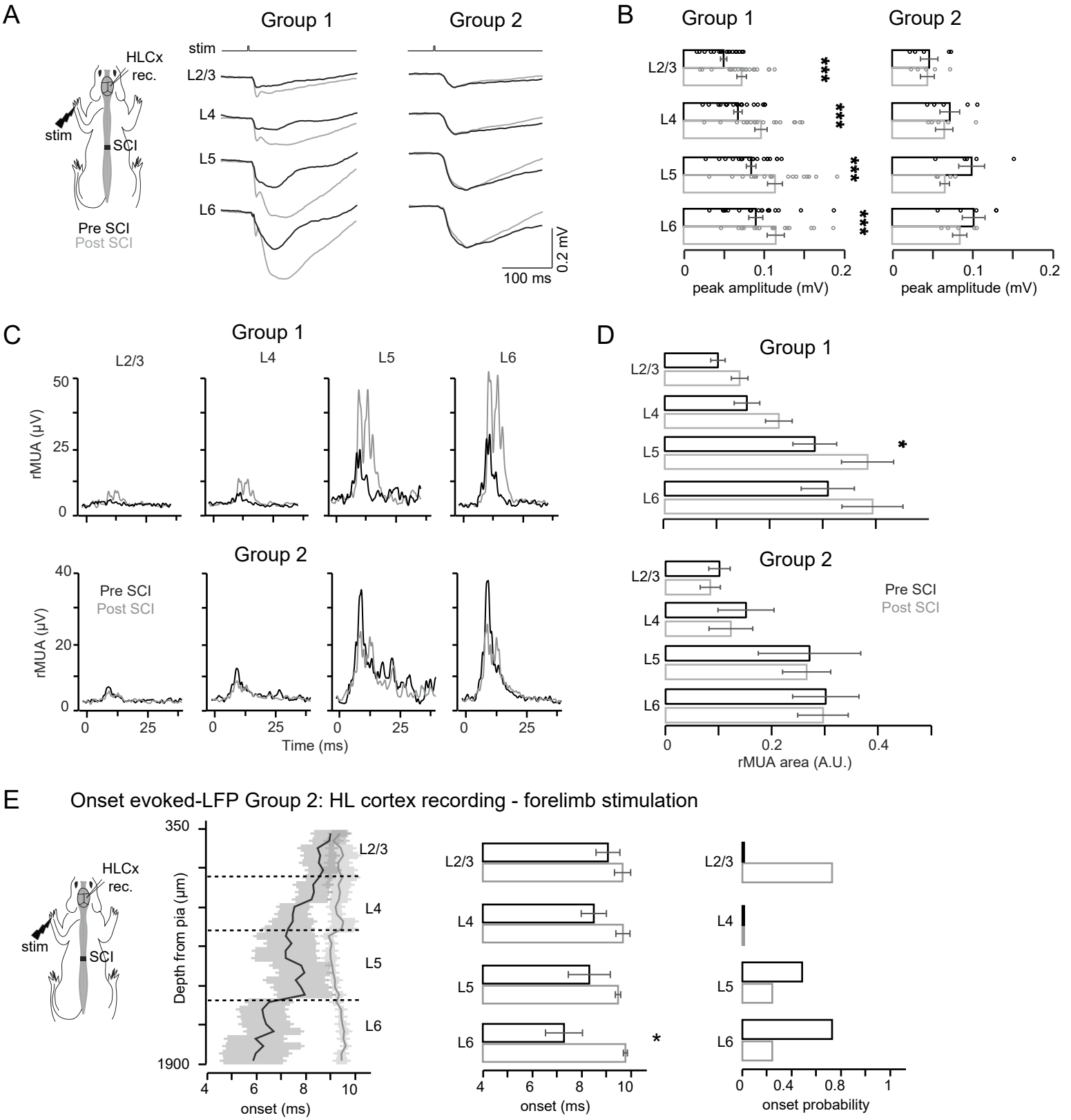


*Supplemental Figure 1: Evoked-responses after SCI in the two-subgroups.* (A) Scheme of a SCI animal recording of HLCx (rec.) and forelimb stimulation (FL stim) and examples of averaged evoked-LFP recorded in HLCx in response to FL stim (5 mA) before (black) and after SCI (grey) in group 1 and 2. (B) Population average of the evoked-LFP amplitude from animals across layers before and after SCI in group 1 and 2. (C) Examples of averaged evoked-rMUA recorded in HLCx in response to FL stim (5 mA) before and after SCI in group 1 and 2. (D) Population average of the evoked-rMUA area from animals across layers before and after SCI in group 1 and 2. (E) Averaged LFP-onset laminar profile of HLCx in response to forelimb stimulation at 5 mA in Group 2. Left, laminar profile of the whole cortical column. Middle: bar graph showing population averaged onset responses across layers. Right, normalized histogram showing onset probability across layers. Data are mean ± sem (n = 19 for LFP-group 1, 5 for LFP-group 2, 16 for rMUA-group 1 and 3 for rMUA-group 2). * $p < 0.05$, ** $p < 0.01$, *** $p < 0.001$. Related to Figure 2 and Figure 4.

**Supplementary Table 1: Related to Figure 1, Evoked responses in HLCx by hindlimb and forelimb stimulation.** One-way Analysis of Variance (ANOVA) for control responses. Tukey post hoc comparisons are shown for significances $p < 0.05$.

| | Limb stimulated | Intensity (mA) | Layer effect | *Post-hoc* Tukey ($p<0.05$) |
|---|---|---|---|---|
| LFP amplitude | HL | 0.5 | $F_{(3,89)}=0.9$<br>$p=0.46$ | |
| | | 5 | $F_{(3,89)}=6.7$<br>$p<0.001$ | L2/3 vs L6; $p=0.048$<br>L4 vs L6; $p<0.001$ |
| | FL | 0.5 | $F_{(3,92)}=4.1$<br>$p=0.009$ | L2/3 vs L5; $p=0.007$<br>L2/3 vs L6; $p=0.045$ |
| | | 5 | $F_{(3,92)}=12.1$<br>$p<0.001$ | L2/3 vs L5; $p<0.001$<br>L2/3 vs L6; $p<0.001$<br>L4 vs L6; $p=0.024$ |
| rMUA area | HL | 0.5 | $F_{(3,60)}=2.6$<br>$p=0.062$ | |
| | | 5 | $F_{(3,60)}=26$<br>$p<0.001$ | L2/3 vs L4; $p<0.001$<br>L2/3 vs L5; $p<0.001$<br>L2/3 vs L6; $p=0.005$<br>L4 vs L5; $p<0.001$<br>L5 vs L6; $p<0.001$ |
| | FL | 0.5 | $F_{(3,60)}=6.2$<br>$p<0.001$ | L2/3 vs L5; $p=0.004$<br>L2/3 vs L6; $p=0.033$<br>L4 vs L5; $p=0.014$ |
| | | 5 | $F_{(3,60)}=9.5$<br>$p<0.001$ | L2/3 vs L5; $p=0.002$<br>L2/3 vs L6; $p<0.001$<br>L4 vs L5; $p=0.026$<br>L4 vs L6; $p=0.01$ |

**Supplementary Table 2. Related to Figure 2 and 3, Evoked responses in deafferented HLCx by forelimb stimulation.** Two-way repeated measures Analysis of Variance (ANOVA) for comparisons between pre- and post-lesion responses across layers when forelimb was stimulated. Post hoc significance is described just for comparisons between conditions in the same layer (lesion effect).

| | Group | mA | Lesion effect | Layer effect | Lesion* Layer effect | *Post-hoc* Tukey |
|---|---|---|---|---|---|---|
| LFP amplitude | All | 0.5 | $F_{(1,92)}=51.8$ $p<0.001$ | $F_{(3,92)}=3.2$ $p=0.026$ | $F_{(3,92)}=0.2$ $p=0.92$ | L2/3 p=0.055<br>L4 p=0.006<br>L5 p=0.003<br>L6 p=0.015 |
| | | 5 | $F_{(1,91)}=50.2$ $p<0.001$ | $F_{(3,91)}=10.3$ $p<0.001$ | $F_{(3,91)}=0.3$ $p=0.8$ | L2/3 p=0.023<br>L4 p=0.002<br>L5 p=0.005<br>L6 p=0.113 |
| rMUA area | All | 5 | $F_{(1,60)}=18.1$ $p<0.001$ | $F_{(3,60)}=12.5$ $p<0.001$ | $F_{(3,60)}=1.2$ $p=0.3$ | L2/3 p=1<br>L4 p=0.644<br>L5 p=0.038<br>L6 p=0.131 |
| LFP amplitude | Group 1 (79%) | 0.5 | $F_{(1,72)}=48.5$ $p<0.001$ | $F_{(3,72)}=2.3$ $p=0.085$ | $F_{(3,72)}=0.2$ $p=0.9$ | L2/3 p=0.092<br>L4 p=0.014<br>L5 p=0.005<br>L6 p=0.015 |
| | | 5 | $F_{(1,72)}=125$ $p<0.001$ | $F_{(3,72)}=7$ $p<0.001$ | $F_{(3,72)}=0.5$ $p=0.68$ | L2/3 p<0.001<br>L4 p<0.001<br>L5 p<0.001<br>L6 p<0.001 |
| rMUA area | Group 1 (79%) | 5 | $F_{(1,47)}=25.5$ $p<0.001$ | $F_{(3,47)}=9.5$ $p<0.001$ | $F_{(3,47)}=1$ $p=0.4$ | L2/3 p=0.91<br>L4 p=0.575<br>L5 p=0.015<br>L6 p=0.064 |
| LFP amplitude | Group 2 (21%) | 0.5 | $F_{(1,16)}=4.5$ $p=0.05$ | $F_{(3,16)}=0.8$ $p=0.5$ | $F_{(3,16)}=0.1$ $p=0.95$ | |
| | | 5 | $F_{(1,15)}=15.2$ $p=0.001$ | $F_{(3,15)}=4.2$ $p=0.03$ | $F_{(3,15)}=1.8$ $p=0.2$ | L2/3 p=1<br>L4 p=0.908<br>L5 p=0.116<br>L6 p=0.122 |
| rMUA area | Group 2 (21%) | 5 | $F_{(1,8)}=0.5$ $p=0.5$ | $F_{(3,8)}=4.1$ $p=0.05$ | $F_{(3,8)}=0.1$ $p=0.97$ | |

**Supplementary Table 3: Related to Figure 7, Frequency content across layers of HLCx before and immediately after a SCI.** Two-way Analysis of Variance (ANOVA) of the relative power spectrum of each band frequency in the spontaneous activity fast transform fourier analysis. Post hoc significance is described just for comparisons between conditions in the same layer (lesion effect). Analysis from Group 1 animals.

| | Lesion effect | Layer effect | Lesion*Layer effect | Post hoc Tukey |
|---|---|---|---|---|
| SWA | $F_{(1,54)}$=5.5<br>p=0.023 | $F_{(3,54)}$=2.1<br>p=0.136 | $F_{(2,54)}$=0.2<br>p=0.82 | L2/3 p=0.95<br>L4 p =0.49<br>L5/6 p=0.73 |
| Delta | $F_{(1,54)}$=3.5<br>p=0.067 | $F_{(3,54)}$=0.9<br>p=0.412 | $F_{(2,54)}$=0.3<br>p=0.76 | |
| Theta | $F_{(1,54)}$=8.9<br>p=0.004 | $F_{(3,54)}$=10.4<br>p<0.001 | $F_{(2,54)}$=0.1<br>p=0.9 | L2/3 p=0.352<br>L4 p=0.493<br>L5/6 p=0.741 |
| Alfa | $F_{(1,51)}$=8.9<br>p=0.02 | $F_{(3,51)}$=31.1<br>p<0.001 | $F_{(2,51)}$=0.3<br>p=0.75 | L2/3 p=0.53<br>L4 p=0.97<br>L5/6 p=0.58 |
| Beta | $F_{(1,51)}$=2.7<br>p=0.1 | $F_{(3,51)}$=28<br>p<0.001 | $F_{(2,51)}$=0.1<br>p=0.9 | |
| Low gamma | $F_{(1,51)}$=4.9<br>p=0.031 | $F_{(3,51)}$=15.8<br>p<0.001 | $F_{(2,51)}$=1.3<br>p=0.27 | L2/3 p=0.112<br>L4 p=0.991<br>L5/6 p=0.988 |
| High gamma | $F_{(1,51)}$=8.6<br>p=0.005 | $F_{(3,52)}$=11.7<br>p<0.001 | $F_{(2,52)}$=3.3<br>p=0.046 | L2/3 p=0.006<br>L4 p=0.923<br>L5 p=0.999 |